CHARACTERIZATION OF LABORATORY-AND FIELD-COMPACTED ASPHALT MIXTURES BASED ON DYNAMIC MODULUS TESTING AND ANALYSIS

A Thesis

by

LEELA SUSHITHA CHINNAKOTLA

Submitted to the Office of Graduate and Professional Studies of
Texas A&M University
in partial fulfillment of the requirements for the degree of

MASTER OF SCIENCE

Chair of Committee,	Bjorn Birgisson
Committee Members,	Robert Lytton
	Zofia Rybkowski
Head of Department,	Robin Autenrieth

May 2021

Major Subject: Civil Engineering

ABSTRACT

This first part of the thesis investigates a fast, non-destructive testing method to characterize asphalt mixtures. While dynamic modulus was recommended by NCHRP Project 9-19 as a test to represent pavement performance, the time consumed by the commonly used cyclic test method hampers its adaptation. The possibility of using the resonance test method for determining the complex modulus in a quicker, simpler, and reliable way was evaluated to address this gap. For comparison purposes, complex modulus testing was performed on two asphalt mixtures using the cyclic loading and the resonance frequency methods. The results plotted in Cole-Cole space show that the measurements from both the tests are consistent. The AASHTO R 84 and Havriliak-Negami models were used to estimate the master curves of dynamic modulus and phase angle. The AASHTO R 84 standard procedure could not be extended to fit the resonance test measurements.

The second part assesses a new optimum asphalt mixture design procedure using the proposed micromechanics-based performance indicator. The original Superpave mixture design relies only on the material specifications and volumetrics criteria to ensure satisfactory mixture performance. Also, to better predict the asphalt mixture performance, understanding the influence of individual mixture components is necessary along with the effective bulk properties, which is often overlooked. These two shortcomings in the current asphalt mixture design procedure were addressed in this thesis by introducing a new performance indicator. The prediction equations from a micromechanical framework developed by Onifade and Birgisson (2021) were used to find the mixture constituents' modulus. The microstructure characteristics like the volume fraction of

phases, the shape and texture of aggregates, and the arrangement of constituents are also incorporated within the equations used. Based on the predicted stiffness values of the mixture and the constituents, a performance parameter termed the mixture/mastic stiffness ratio is introduced. This parameter can provide preliminary analysis indicating the rutting and fatigue performance of a mixture design without the need for extensive testing. The stiffness ratios correlated well with flow number and critical strain energy at the test temperature and frequency. Further, the ratio was sensitive to mixture gradation and aging.

ACKNOWLEDGMENTS

I sincerely thank my advisor Prof. Bjorn Birgisson for his immense support, guidance, and motivation. Throughout the span of my thesis, he has been extremely encouraging and understanding, which enabled me to hold my confidence at every phase of my master's degree. I would be forever grateful to him for believing in me and involving me in this innovative project.

I would like to extend my thanks to Prof. Robert Lytton and Dr. Zofia Rybkowski for accepting to join me as my thesis committee members and extending their time, support, and patience.

This thesis would not have been possible without the support of Dr. Ibrahim Onifade, who stayed as my mentor at both academic and personal levels throughout. He not only helped me understand numerous concepts from the foundation level but also instilled in me a proper research approach.

I would also like to thank Dr. Kai Huang for planning the material preparation and helping me immensely in the laboratory.

Finally, I would like to express my gratitude to my family and friends for their unwavering support and encouragement.

CONTRIBUTORS AND FUNDING SOURCES

Contributors

This work was supported by a thesis committee consisting of Professor Bjorn Birgisson [advisor] and Professor Robert Lytton of the Department of Civil and Environmental Engineering, and Associate Professor Zofia K. Rybkowski of the Department of Construction Science, Center for Health Systems and Design.

The code used for the analysis in Chapter IV was provided by Doctor Ibrahim Onifade. The test data analyzed in Chapter V was measured by Joint Transportation Research Program and was published in 2015 as report FHWA/IN/JTRP-2015/25.

All other work conducted for the thesis was completed by the student independently.

Funding Sources

Graduate study was supported by a fellowship from Texas A&M University and funding from the Swedish Transport Administration.

TABLE OF CONTENTS

Page

LIST OF FIGURES

Page

Page

Page

LIST OF TABLES

Page

Page

CHAPTER I

INTRODUCTION AND LITERATURE REVIEW

Background

Asphalt mixtures are multiphase particulate composite systems composed of aggregate, binder, and air voids. Although 95 percent by weight of asphalt mixtures is made up of aggregate with only 5 percent asphalt binder, the performance of a mixture is significantly influenced by the characteristics of the binder. The key performance properties of asphalt mixtures include the potential for resisting permanent deformation, fatigue cracking, and low-temperature cracking. The presence of an asphalt binder combined with a high proportion of granular materials makes the asphalt mixture time-, temperature-dependent, as well as stress-dependent. The resulting asphalt mixture exhibits viscoelastic responses when subjected to loading. Hence, understanding the behavior and response of asphalt mixtures under external stimuli of traffic loads requires accurate characterization of pavement materials.

According to viscoelastic theory, the non-destructive properties of the mixtures can be characterized by creep compliance, relaxation modulus, dynamic modulus, and phase angle (Zhang 2012). Of these, complex modulus (E*) is a prevalently used measure while conducting pavement mixture evaluation. The E* is a complex number containing both storage (real) and loss (imaginary) modulus. The absolute modulus of the complex modulus is the dynamic modulus, identified by |E*|. Coffman and Pagen originally developed the test protocol for determining the dynamic modulus for asphalt materials in the 1960s (Williams 2015). The idea was to subject the material under either compressive or tensile sinusoidal stress in a uniaxial direction and measure the resulting strain. It was then developed as a standard in 1979 with the designation D3497 in ASTM standards and TP62 in AASHTO specifications. According to NCHRP report 513

(Bonaquist 2003), the dynamic modulus correlates well with field permanent deformation behavior and integrates with the Superpave system framework for performance evaluation. Currently, the dynamic modulus is one of the most critical parameters needed in the Mechanistic-Empirical Pavement Guide (MEPDG) (Bennert 2009). The design procedure uses a dynamic modulus master curve for determining the structural capacity of pavement through both rutting and fatigue cracking distress predictions.

Further, the development of Asphalt Mixture Performance Tester (AMPT) has simplified the generation of master curves needed for mechanistic-empirical structural design (FHWA 2013). After several studies in the NCHRP Project 9-19 and NCHRP Project 9-29, the AMPT is presently the most used test equipment for determining the dynamic modulus of asphalt mixtures by the Transportation Agencies and the universities in the United States. Since both dynamic modulus and flow number (an indicator of flexible pavement rutting resistance) can be performed using the same test equipment, the AMPT provides a link between mixture design and structural analysis.

However, over the past two decades, several issues were identified with the use of AMPT for dynamic modulus testing. A few of them include (Zhang et al. 2013):

a) Lengthy test time of nearly a week (Dougan et al. 2003),
b) Requires long wait periods for the temperature to reach equilibrium, especially at temperatures below 5ºC,
c) Problematic maintaining the Linear Variable Differential Transformer (LVDT) studs at high temperatures as they are stuck to the mixture with meltable adhesive,
d) Requires a heavy setup that cannot be moved easily,
e) Not ideal for routing mix-design and screening,
f) Inability to readily test field cores or samples with different dimensions,

g) High variability of the test results (Daniel et al. 2004, Bhasin et al. 2003).

Other equipment that performs cyclic loading also has similar problems. Dougan et al. (2003) conducted an extensive study for 30 months to identify the problems encountered while implementing the cyclic test protocol and suggest remedies. They categorized the issues into four sections: a) protocol, b) specimen preparation, c) conducting the E* test, and d) presentation of results. Some of the important concerns include difficulty in compacting the sample to desired dimensions, unable to achieve temperature equilibrium between the chamber and the specimen in a short period, condensation of moisture inside the test chamber, and requirement to maintain the axial strain below 150 micro strains.

In order to bypass these difficulties in dynamic modulus testing, the application of wave methods like resonance and ultrasonic testing to asphalt mixtures has gained popularity. The ASTM C215 standard for concrete limits the E* calculation through impact resonance test to one or two resonant frequencies and with sample geometries with $L/D > 2$ or $L/D < 0.25$. As initial attempts, applying the standard to asphalt mixtures resulted in repeatable results for long cylinders of $L/D > 2$ (Whitmoyer and Kim 1994). The same standard was again used by Kweon and Kim (2006) on asphalt mixtures but with correction factors accounting for the damping and the specimen geometry. Boz (2016) utilized the impact resonance test to characterize the properties of asphalt mixtures and recycled asphalt pavement binder. He observed that the impact resonance test was influenced by specimen size and test configuration. However, small variations in the specimen dimensions do not substantially affect the dynamic modulus values (Tauste et al. 2017). The resonance test performed on prismatic specimens showed that the damping of the vibration had a significant impact on the test. The accuracy of the method also depended on the temperature and the type of binder used. However, all these studies were performed at one resonance frequency for

a given temperature. Significant improvements in the usage of resonance testing for asphalt mixtures were made by Ryden (2009) and Gudmarsson (2014), who applied three-dimensional numerical calculations to estimate the complex modulus at many different frequencies and on any sample size.

Larcher et al. (2015) applied ultrasonic p-waves to determine wave propagation parameters at frequencies between 200 kHz to 300 kHz and temperatures from -20ºC to 40ºC. By considering a 2D propagation of waves in an isotropic viscoelastic medium, the high-frequency complex modulus and its components were computed based on the wave velocity and attenuation factor. Though accurate results were obtained fitting into the 2S2P1D model, they observed that the test yielded high frequencies not suitable for current pavement design practice. Norambuena-Contreras et al. (2010) demonstrated the potential for replacing the standard low-frequency dynamic modulus testing with direct ultrasonic testing by multiplication of a correction factor to the calculated high-frequency modulus.

Bekele et al. (2019) attempted to automate the fundamental resonant frequency measurement by using a loudspeaker set up in the thermal chamber and excite the asphalt specimens remotely. Since the measurement was controlled by a computer in non-contact mode with the specimen placed within the thermal chamber, the technique eliminated thermal disturbances.

However, there is still a need for more literature to emphasize the use of these methods for faster and reliable non-destructive laboratory testing. Moreover, these methods include post-computational analysis of the test data for obtaining the desired pavement properties (dynamic modulus, phase angle, and Poisson's ratio). Thus, more research is required to understand the dynamics of these tests, select suitable optimization techniques, assess the sensitivity and

repeatability of the test procedures, and compare the results with the existing conventional methods.

In general, the stiffness of asphalt mixture and the stiffness of mixture constituents like mastic stiffness are studied separately and linked with the pavement performance (Abbas et al. 2004, Droogers 2018). However, a recent study by Onifade and Birgisson (2021) found that the stiffness contrast between the mixture constituents strongly influences the load transfer in the mixture. Hence, it is essential to consider both the effective properties and the contribution of the constituents simultaneously for obtaining a realistic picture of asphalt mixture behavior.

Research Objectives

This research tries to resolve the problems mentioned in the section above with three main objectives:

1) To measure the complex modulus of asphalt mixtures through cyclic and resonance tests in the laboratory.
2) To evaluate the individual stiffnesses of mixture components and determine the stiffness ratio between the mixture and the mastic stiffnesses.
3) To relate the effect of mixture components on pavement performance through the stiffness ratio.

CHAPTER II

DYNAMIC MODULUS TESTING OF ASPHALT MIXTURES

Introduction

Dynamic modulus |E*| is a fundamental property of viscoelastic asphalt mixtures that defines the stiffness characteristic as a function of temperature and loading rate. The elastic and viscous behavior of an asphalt mixture is expressed by the complex modulus E*.

For conventional cyclic loading, E* is the ratio of the amplitude of the sinusoidal stress to the amplitude of the sinusoidal strain at any given time t, and angular load frequency ω and steady-state. The dynamic modulus is the absolute value of this complex number calculated according to the following relations (Equation 2-1). The phase angle is quantified by the time lag between the peak stress and peak strain within one load cycle. For purely elastic material, $\delta = 0^o$, and for purely viscous material, $\delta = 90^o$.

$$E^* = \frac{\sigma}{\varepsilon} = \frac{\sigma_o sin\omega t}{\varepsilon_o \sin(\omega t - \delta)} = E' + iE''$$

$$|E^*| = \frac{\sigma_o}{\varepsilon_o}, \delta = tan^{-1}\left(\frac{E''}{E'}\right) \quad \textbf{(2-1)}$$

where E* is the complex modulus, E' is the storage modulus representing elastic energy, E" is the loss modulus representing viscous energy, δ is the phase angle in degrees, σ_o is the peak stress, ε_o is the peak strain, ω is the angular frequency, and t is the time.

In this study, two test methods were followed to obtain the dynamic modulus of the asphalt mixtures at a wide range of temperatures and frequencies a) Cyclic Testing, b) Resonance Testing. The dynamic modulus and phase angle measurements from both the tests are presented and compared below.

Materials

Two dense graded asphalt mixture designs were prepared with the same aggregate gradation and varying binder type. The binders were labeled as AAD and AAM from the Strategic Highway Research Program Materials Reference Library (Jones 1993). The AAD binder was PG 58-28, and the AAM binder was PG 58-22. Lab mixed lab compacted specimens were fabricated with three replicates for each binder type. The air void content was chosen as 4 percent, and the aggregate gradation is shown in Table 2-1. The optimum asphalt content was calculated as 5.01 percent for both the mixtures. All the mixtures were compacted to cylindrical specimens of 150 mm in diameter and 175 mm in height using the Superpave gyratory compactor. They were then cored to 100 mm in diameter and sawed to 150 mm in height. The mixing and compaction temperatures were set to 135ºC and 121ºC, respectively. The volumetrics of the specimens are given in Table 2-2.

Table 2-1 Asphalt Mixtures Gradation and Combined Aggregate Specific Gravity

Sieve Size, mm	% Passing
12.5	100
9.5	99.24
4.75	63.84
2.36	38.20
0.6	16.84
0.3	11.71
0.075	3.30
G_{sb}	2.609

Table 2-2 Asphalt Mixtures Volumetrics

Specimen ID	V_a, %	G_{mb}	VMA, %	VFA, %	P_{be}, %	Dust Ratio
AAD 1	3.9	2.368	13.77	71.66	4.29	1.96
AAD 2	3.9	2.368	13.79	71.55	4.29	1.96

Table 2-2 Continued

Specimen ID	V_a, %	G_{mb}	VMA, %	VFA, %	P_{be}, %	Dust Ratio
AAD 3	4.1	2.364	13.94	70.68	4.29	1.96
AAM 1	3.8	2.372	13.64	72.49	4.29	1.96
AAM 2	3.8	2.371	13.67	72.28	4.29	1.96
AAM 3	4.1	2.365	13.91	70.85	4.29	1.96

Tests Configurations and Data Analysis

Cyclic Test Method

AASHTO T 378 (2017) describes the method for determining the dynamic modulus of asphalt mixtures using Asphalt Mixture Performance Tester (AMPT). AMPT is a computer-controlled hydraulic testing system that can cyclically load a compacted asphalt mixture specimen over a wide temperature and frequency range (FHWA 2020). Unconfined dynamic modulus test was performed on the specimens covering four temperatures (4.4ºC, 10ºC, 21.1ºC, 37.8ºC) and seven frequencies (0.01 Hz, 0.1 Hz, 0.5 Hz, 1 Hz, 5 Hz, 10 Hz, 25 Hz). The strain range was fixed between 85 to 115 micro-strain following the NCHRP 9-29 default values. The setup consisted of three linear variable differential transformers mounted at 120º from each other with a gauge length of 70 mm. Two rubber membranes were placed between the specimen and the platen to reduce fiction (Figure 2-1). The software linked determines the applied stress and the applied strain using the input values and the recorded deformations. These values are used to provide the mixture dynamic modulus and phase angle at each temperature and frequency.

Figure 2-1 Asphalt Mixture Performance Tester Setup

Resonance Test Method

The resonance frequency method includes three parts: 1) Measurement of the frequency response functions (FRFs), 2) Finite element calculations of FRFs, and 3) Optimization procedure to match calculated and measured FRFs.

The testing was performed through impact excitation (Figure 2-2). Each specimen was laid down along the horizontal direction on a soft foam for free boundary conditions and hit five times at the center of the short side using an impact hammer (PCB model 086E80) to generate a longitudinal (symmetric) mode of vibration. The accelerometer (PCB model 35B10) attached to the other end with an instant adhesive was used to measure the standing wave responses. The hammer and the accelerometer were connected to a signal conditioner (PCB model 086E80), which prepares the signals for analog to digital conversion and amplifies the signals if required. The final signal conversion is performed through a data acquisition device (NI USB-6251 M Series) and stored in a computer connected.

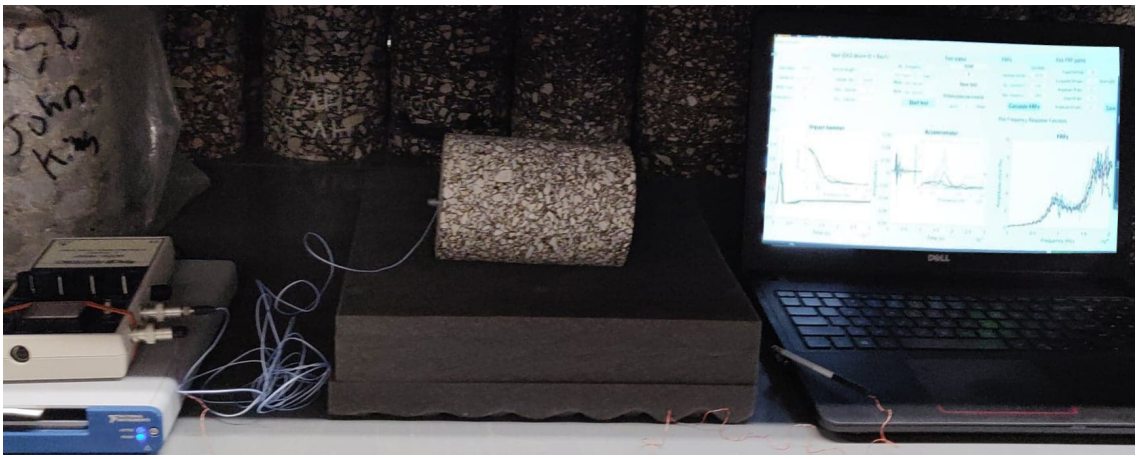

Figure 2-2 Equipment Used to Perform Resonance Testing

A MATLAB application developed by (Gudmarsson 2014a) was used for performing the modal testing. The record length was set to 5 seconds to include all the vibrations of the specimen until completely damped out, and the measurements were recorded with a sampling frequency of 500 kHz. The averaged frequency response function was determined by averaging the five measurements in the complex domain at each frequency according to Equation 2-2.

$$H(f) = \frac{\left(\frac{1}{n}\sum_{k=1}^{n} Y_k(f).X^*_k(f)\right)}{\left(\frac{1}{n}\sum_{k=1}^{n} X_k(f).X^*_k(f)\right)} \quad \textbf{(2-2)}$$

where H(f) is the FRF, Y(f) is the measured acceleration, X(f) is the measured applied force, X*(f) is the complex conjugate of the applied force, n is the number of impacts, and k is the index of impact.

Figure 2-3 shows the interface of the application with the input fields and graphs of measurements in the time and frequency domain. Points were picked based on the first two

resonance peaks of the FRF to reduce the computational time in the stiffness evaluation and increase the accuracy of optimization in part 2.

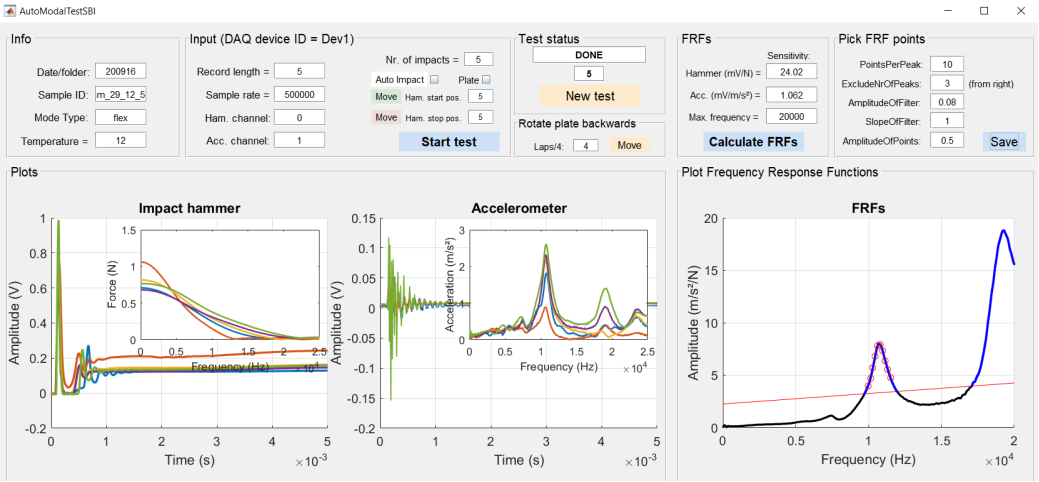

Figure 2-3 Screenshot of Application to Perform Modal Testing

A finite element method (FEM) based COMSOL Multiphysics® application proposed by (Gudmarsson and Ryden 2017) was used to optimize the theoretical FRFs to measured FRFs. The numerical computation of FRFs in a three-dimensional space is detailed in (Gudmarsson et al. 2015). The program applies a point load of 1 N at the center of the cylindrical specimen in a negative z-direction to simulate actual hammer impact. The response in the model is determined in the point corresponding to the accelerometer placement during the measurements. A normal mesh was chosen for all the analyses. Based on the assumed start values of complex modulus E* and complex Poisson's ratio ν^*, the FRFs are calculated and compared with the measured FRFs. The E* and ν^* are adjusted iteratively until these computed and measured FRFs match. Equation 2-3 presents the minimization function to determine the difference between the theoretical and measured FRFs.

$$Error = \sum_{i=1}^{N}\left(\left|H_{MNorm_i}\right| * \left|\frac{\left|H_{M_i}\right|-\left|H_{T_i}\right|}{\left|H_{M_i}\right|}\right|\right) \quad \textbf{(2-3)}$$

where H_{MNorm} is the normalized measured FRF, H_T is the theoretical FRF, H_M is the measured FRF, i is the index of the data point, and N is the number of data points.

The complex behavior of the mixtures is characterized using Havriliak-Negami (HN) model (Equation 2-4). This model not only applies to viscoelastic materials accurately (Hartmann et al. 1994, Havriliak and Negami 1996, Madigosky et al. 2006) but also has the practical advantage of limited fit parameters (Gudmarsson et al. 2015).

$$E^*(\omega) = E_\infty + \frac{(E_0 - E_\infty)}{[1 + (i\omega_r\tau)^\alpha]^\beta}$$
$$v^*(\omega) = v_\infty + \frac{(v_0 - v_\infty)}{[1 + (i\omega_r\tau_v)^\alpha]^\beta} \quad \textbf{(2-4)}$$

where E_o and v_o are the low-frequency values of the modulus and Poisson's ratio, E_∞ and v_∞ are the high-frequency values of the modulus and Poisson's ratio, ω_r is the reduced frequency in rad/sec, α, β are the fitting parameters that govern the width and asymmetry of the loss factor peak, respectively, τ is the relaxation time of the complex modulus, and τ_v is the relaxation time of the complex Poisson's ratio.

The specimens were tested at 4°C, 12°C, and 25°C. The resonance testing used the same specimens as the cyclic testing to allow accurate comparisons between the results. Table 2-3 gives the assumed start values for the optimization of each mixture at a given temperature. Initially, two resonance peaks were considered for the optimization (Figure 2-4). However, it was observed that the theoretical FRFs were not aligning properly with the measured FRFs upon completion of the optimization (Figure 2-5), resulting in higher dynamic modulus values in the 8 kHz to 15 kHz

frequency region. Also, since pavements are exposed to frequencies lower than the ultrasonic frequencies (> 20 kHz), only the first peak was analyzed in this study (Figures 2-6 and 2-7).

Table 2-3 Start Values for Optimizing the FRFs using HN Model

E_0	E_∞	α	β	τ	ν_1
100	45000	0.4	0.3	0.1	0.35

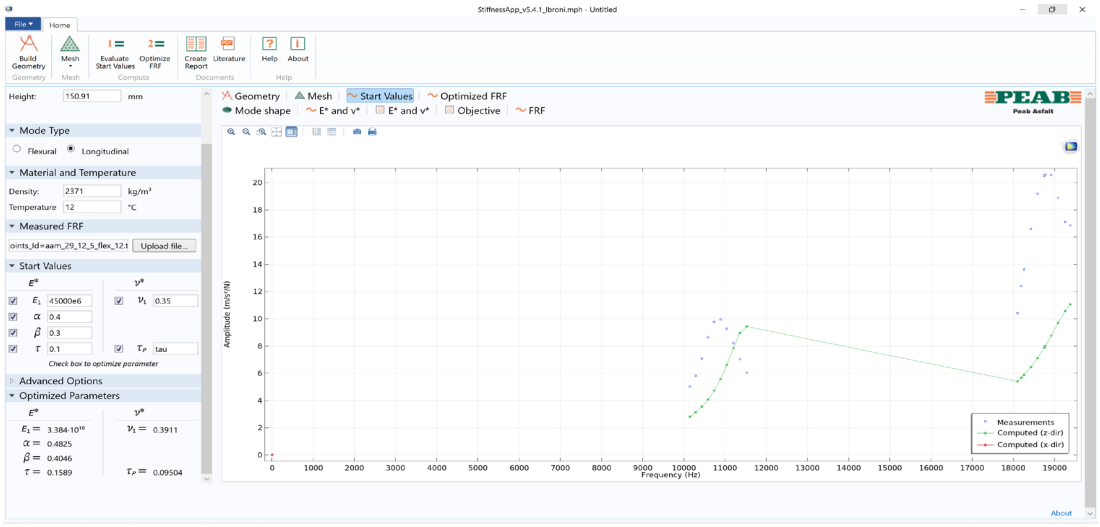

Figure 2-4 Screenshot of the Application with Start Values to Optimize FRFs at Two Resonance Peaks

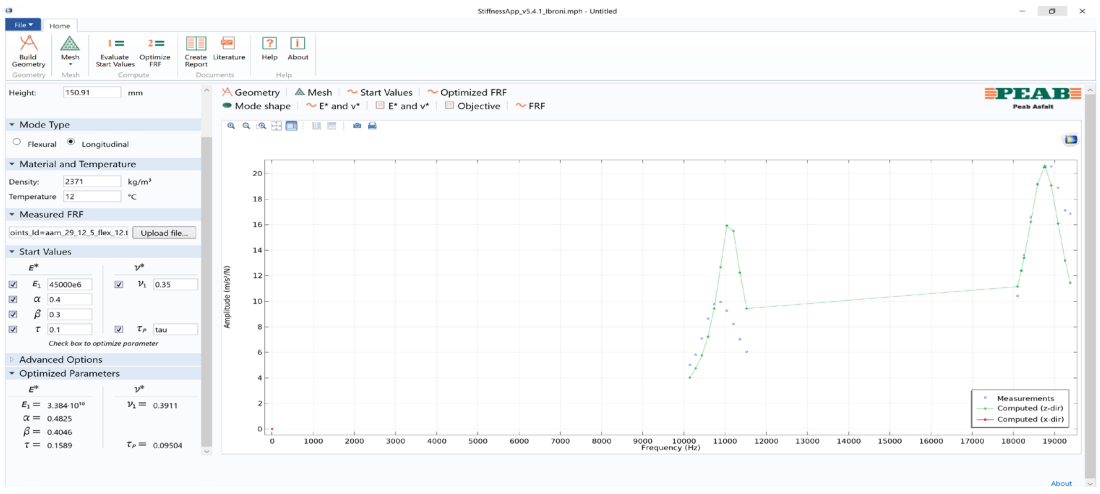

Figure 2-5 Screenshot of the Application with Optimized FRFs at Two Resonance Peaks

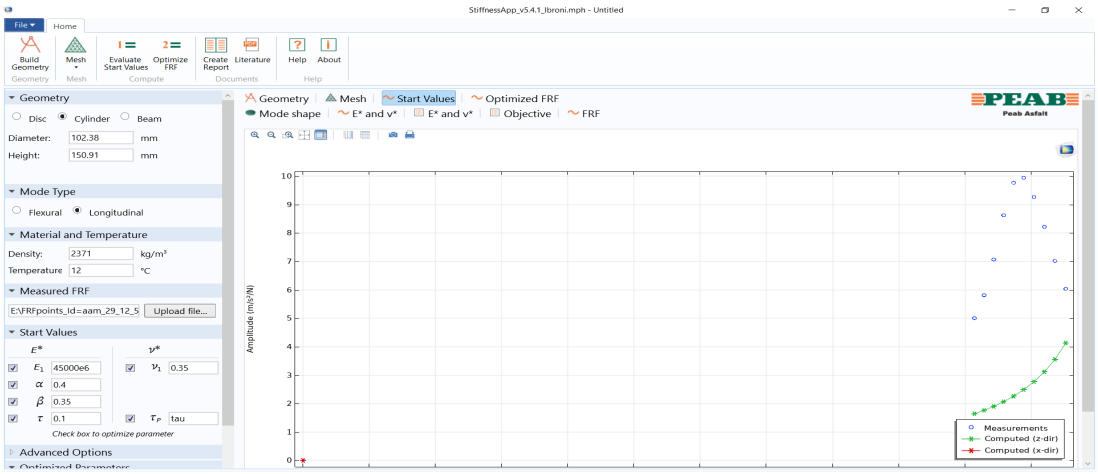

Figure 2-6 Screenshot of the Application with Start Values to Optimize FRFs at One Resonance Peak

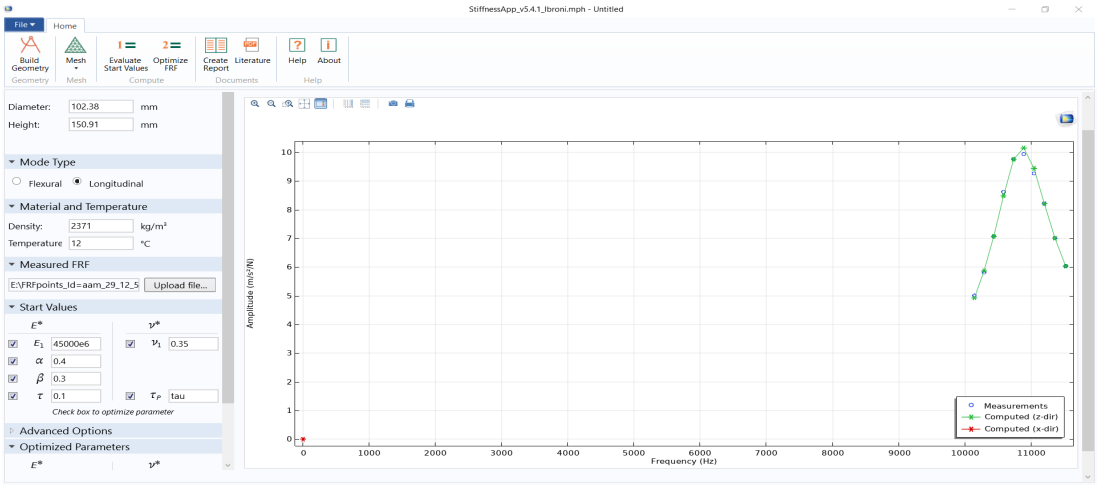

Figure 2-7 Screenshot of the Application with Optimized FRFs at First Resonance Peak

Results

Figure 2-8 and Figure 2-9 shows an example of the dynamic modulus values of a specimen measured through the cyclic test and the resonance test, respectively. In the cyclic test, the properties were observed at discrete low frequencies of 0.01 Hz to 25 Hz at a strain level of 10^{-6} magnitude. While, with the resonance test, the properties were observed at continuous high frequencies of 8 kHz to 20 kHz at strain levels less than 10^{-7} (Gudmarsson et al. 2015). At low

frequencies, given a temperature, the dynamic modulus increased logarithmically with the increase in frequency. While at high frequencies, the rate of change of dynamic modulus reduced drastically. Hence, a nearly linear trend was observed at each test temperature.

The dynamic modulus and the phase angle isotherms of all the mixtures are plotted in Figure 2-10 to Figure 2-21, where "C" represents cyclic test results and "R" represents resonance test results. The phase angle provides insight into how asphalt binder and aggregate structures react when tested at various temperatures and frequencies (Ahmad et al. 2020). At the low-frequency range, the phase angle increased with an increase in frequency up to a peak and further decreased. This is because of the viscoelastic nature of the binder and the interlocking of the aggregates. At high frequency and low temperature, the asphalt binder is stiff and primarily affects the phase angle. As the temperature rises and the frequency drop, the binder weakens, and the aggregate structure starts to affect the phase angle predominantly. At very high frequencies, the phase angle clearly decreased with the increase of frequency at all temperatures due to the elastic nature of the binder.

Based on all the figures, the dynamic moduli from both the tests are nearly falling in the same line for all temperatures measured. But slight inconsistencies were observed in the phase angle measurements. Possible reasons could be that the phase angle measurement through resonance testing was highly dependent on the initial setup of the equipment and the start values during the analysis. A similar issue was reported in (Gudmarsson 2014a), where the amplitude consequently showed higher relative standard deviation (RSD) for the different studies and hence the variations in the loss modulus (phase angle and damping). For better phase angle repeatability, they recommended being meticulous about the accelerometer attachment and the position of the impact and accelerometer. It is more difficult to obtain good phase angle data than good modulus

data (Pellinen et al. 2004, Zhang et al. 2020). Abnormalities were recorded even in the phase angle measurements through the cyclic testing, at low temperature and high frequency (Figures 2-13, 2-17, and 2-19). Bayane et al. (2017) observed a large scatter in the phase angle at high temperatures, measured through the cyclic test. The phase angle was found to be a difficult parameter to determine accurately.

Table 2-4 summarizes the RSD of the two mixture designs based on both the tests. The resonance test had more repeatability in terms of dynamic modulus measurements. But more care had to be taken during the test for achieving better phase angle information. Along with the experimentation errors, these resonance frequency measurements could have varied due to small differences in geometry and potential inhomogeneity within the specimen. Nevertheless, it is easier to improve the quality of the measurements through the resonance test as it is dependent largely on the operator, unlike the cyclic testing, where the variation is mainly due to the instrument.

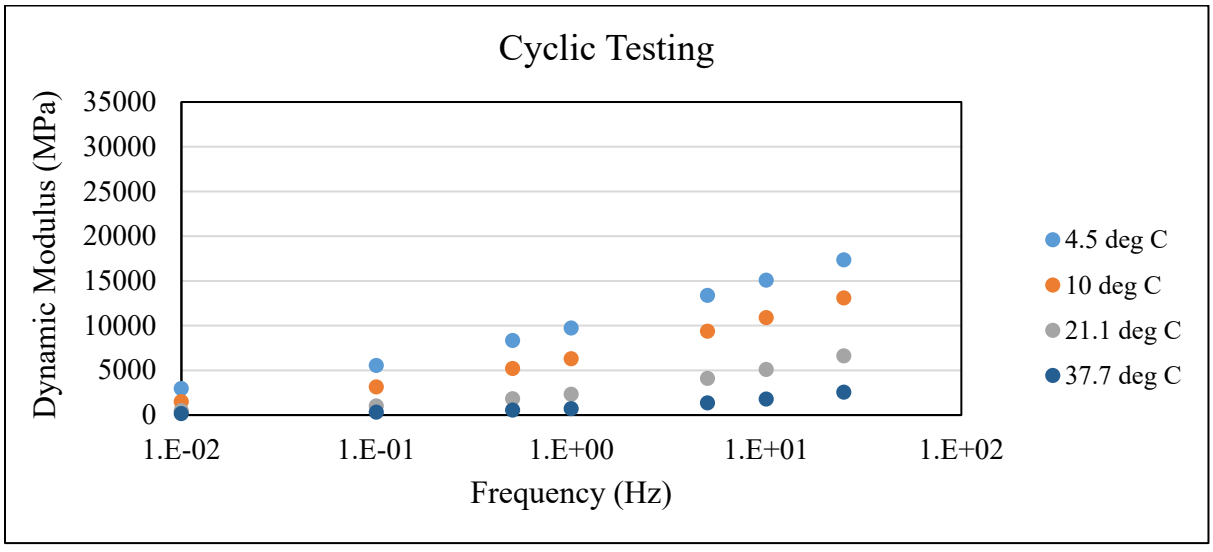

Figure 2-8 Cyclic Test Dynamic Modulus Results

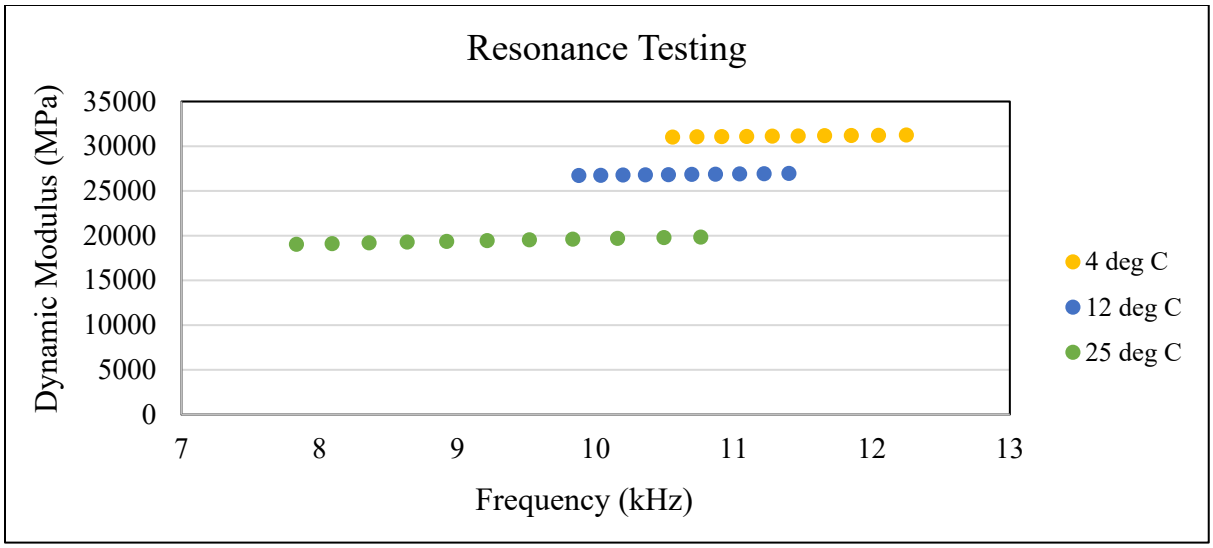

Figure 2-9 Resonance Test Dynamic Modulus Results

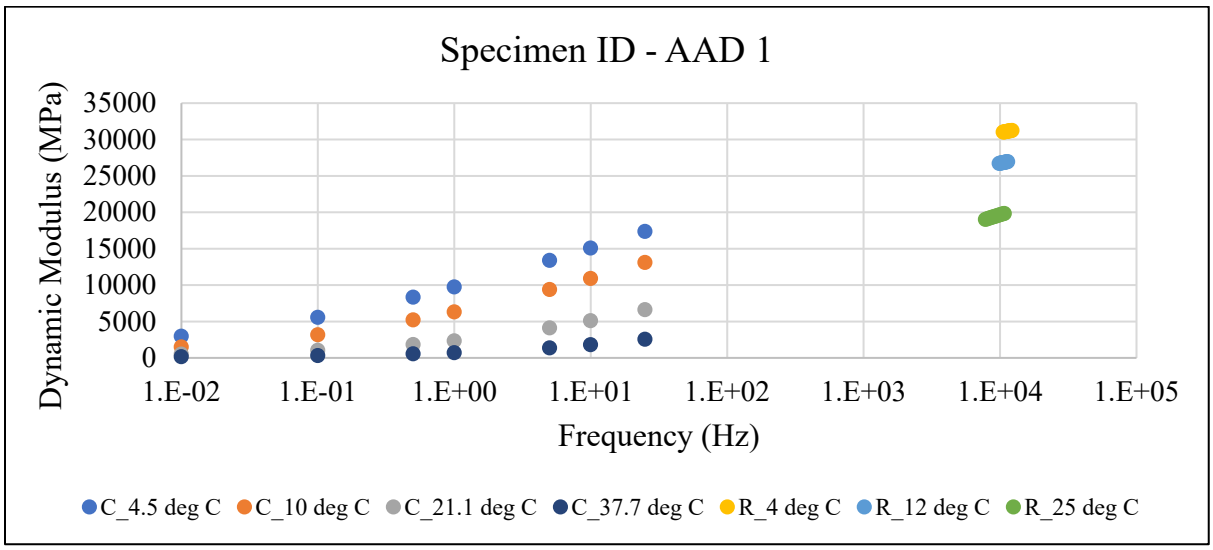

Figure 2-10 Measured Dynamic Modulus Results of the AAD 1 Mixture

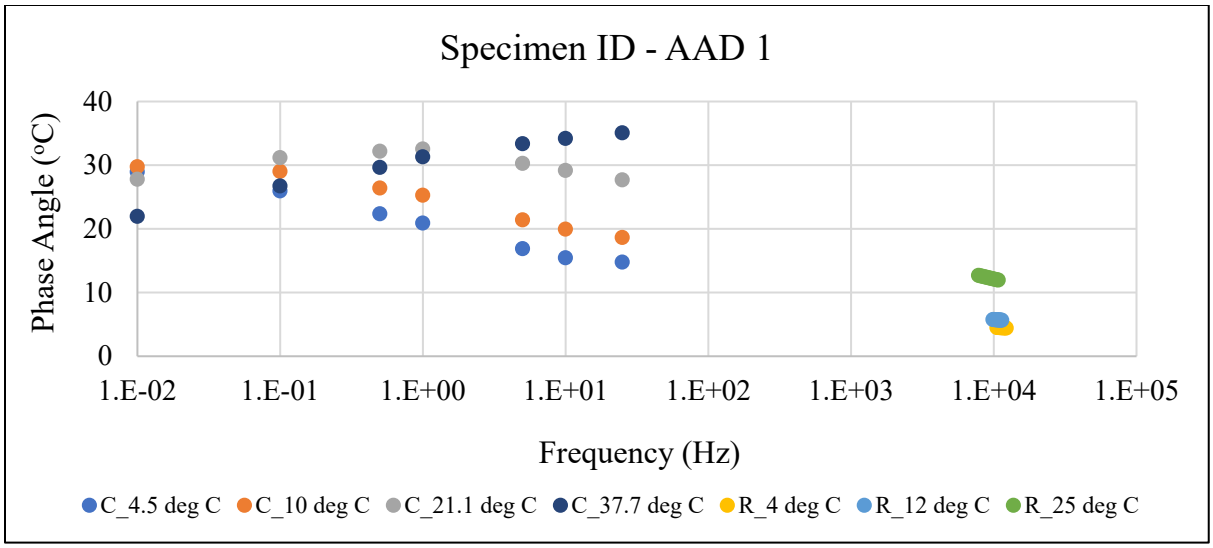

Figure 2-11 Measured Phase Angle Results of the AAD 1 Mixture

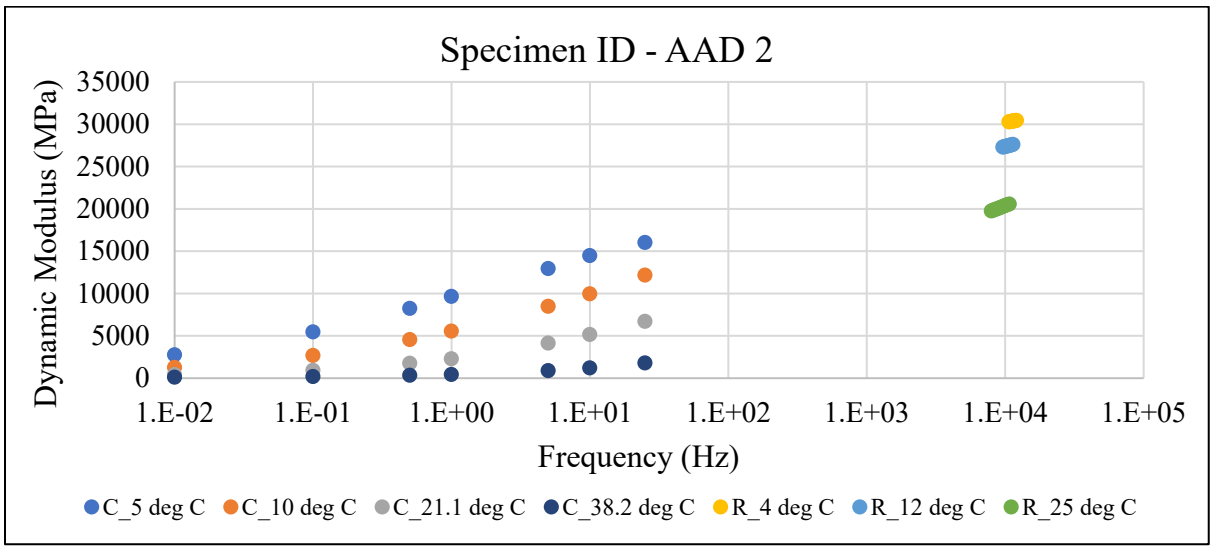

Figure 2-12 Measured Dynamic Modulus Results of the AAD 2 Mixture

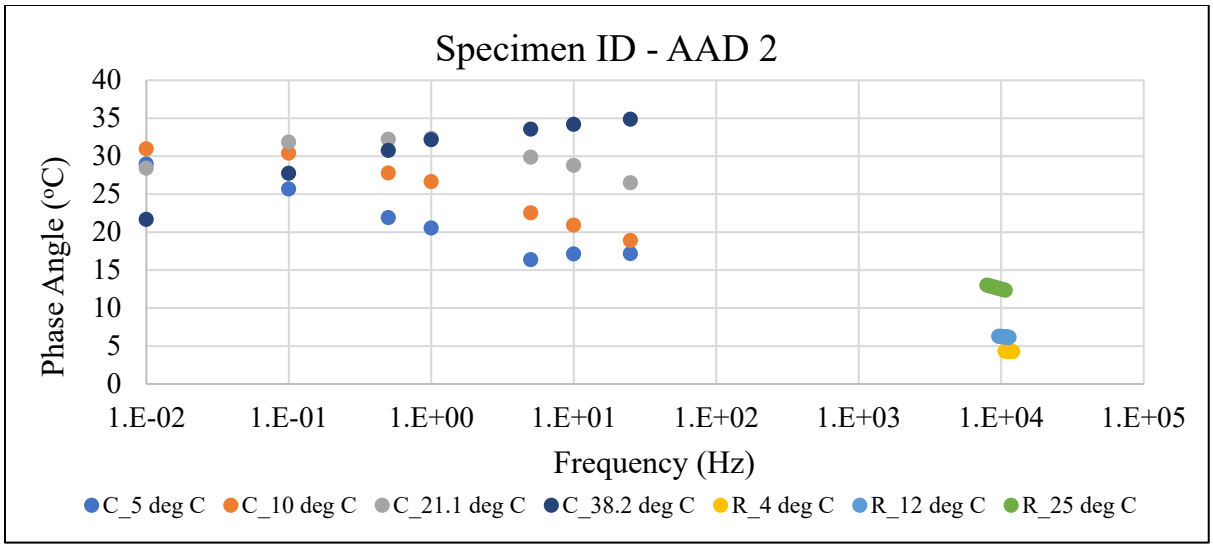

Figure 2-13 Measured Phase Angle Results of the AAD 2 Mixture

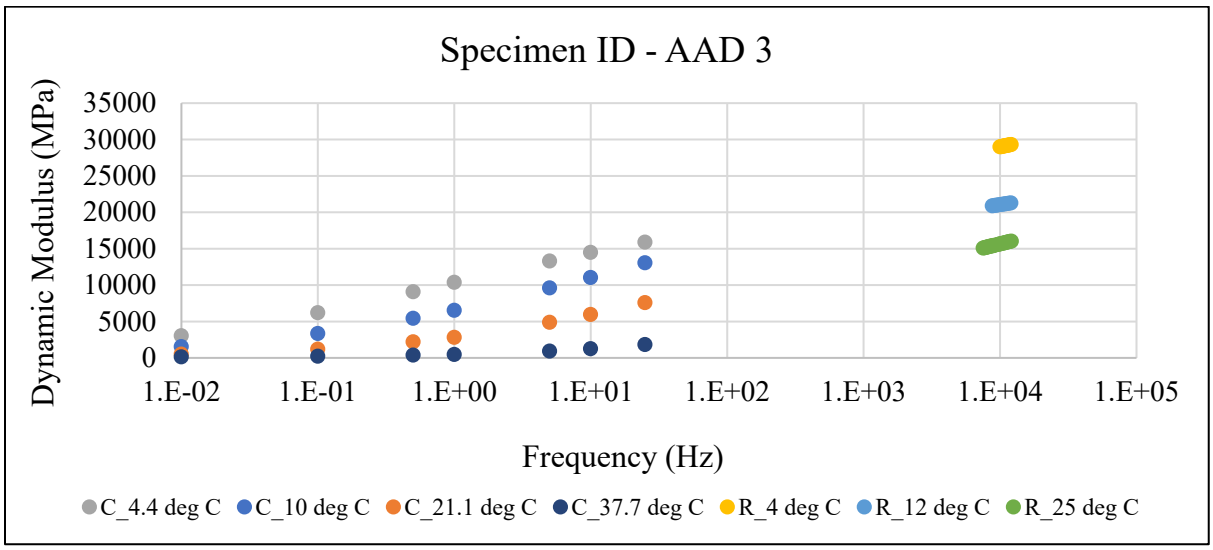

Figure 2-14 Measured Dynamic Modulus Results of the AAD 3 Mixture

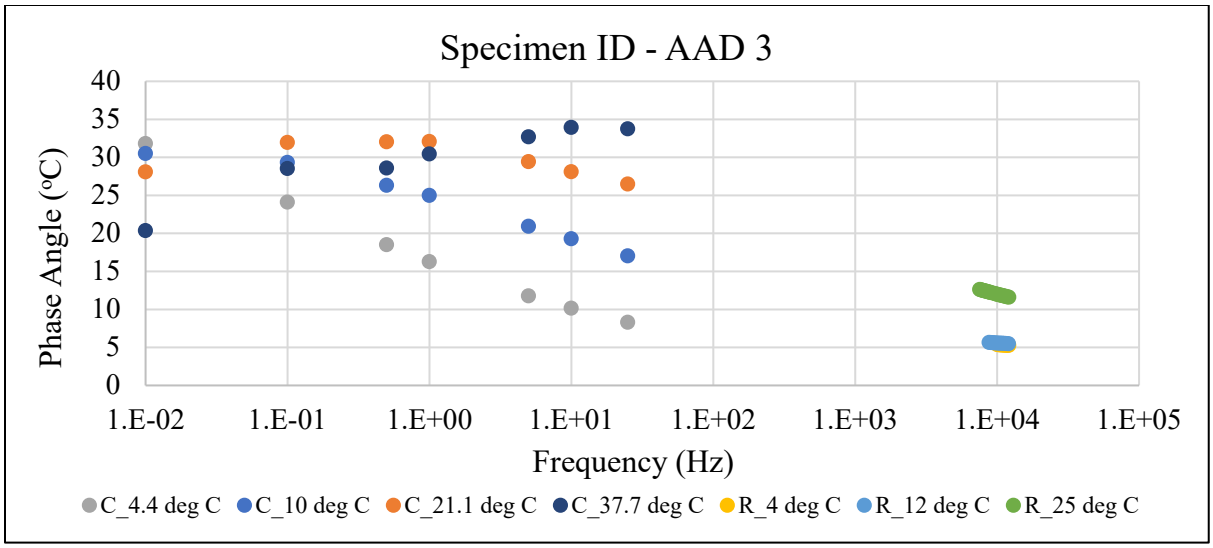

Figure 2-15 Measured Phase Angle Results of the AAD 3 Mixture

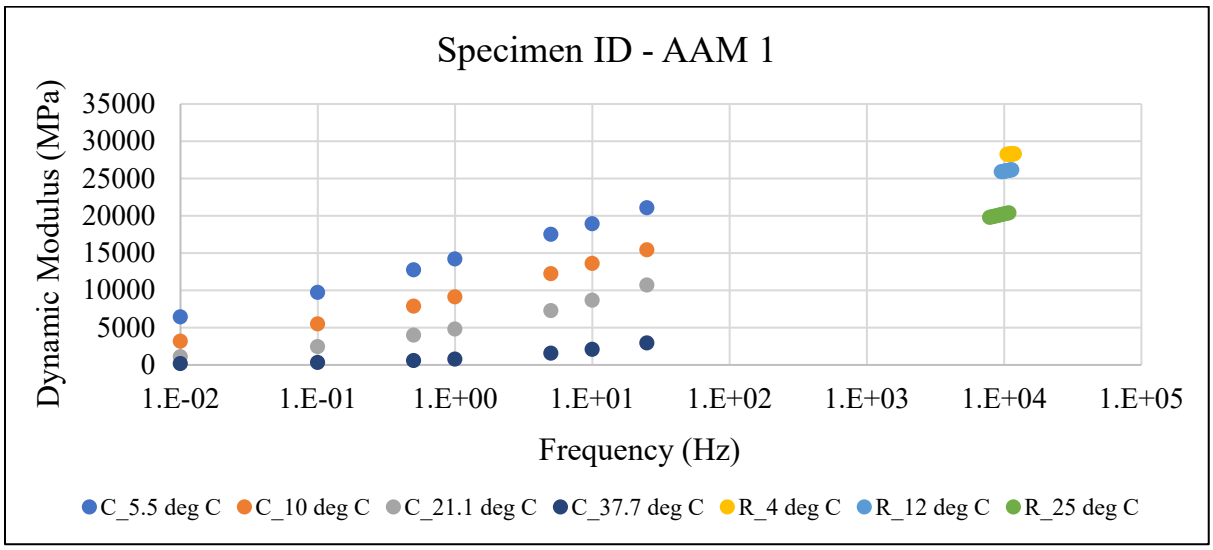

Figure 2-16 Measured Dynamic Modulus Results of the AAM 1 Mixture

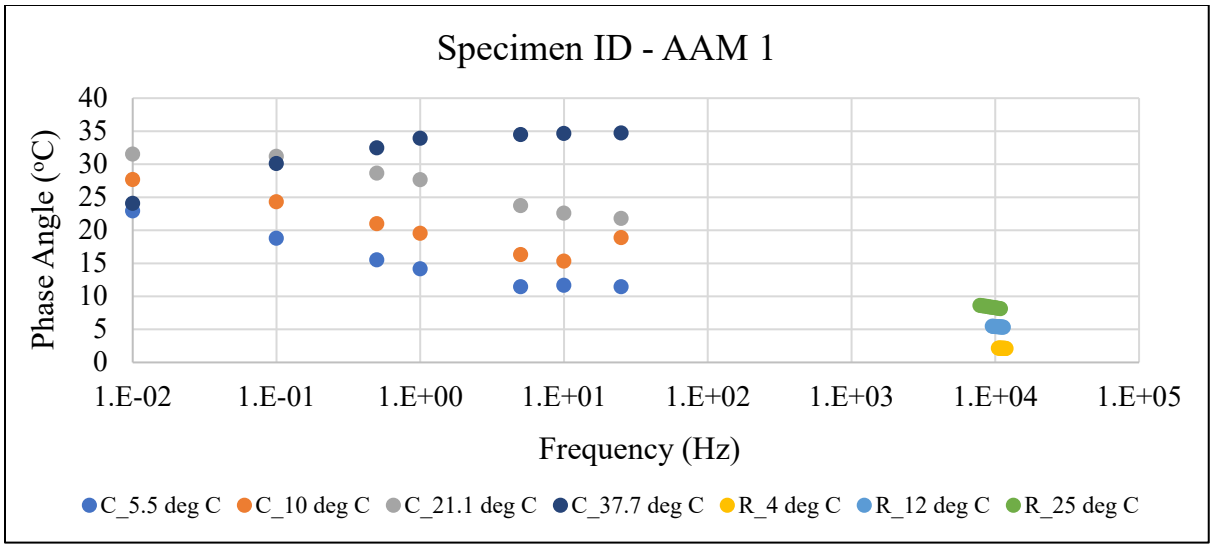

Figure 2-17 Measured Phase Angle Results of the AAM 1 Mixture

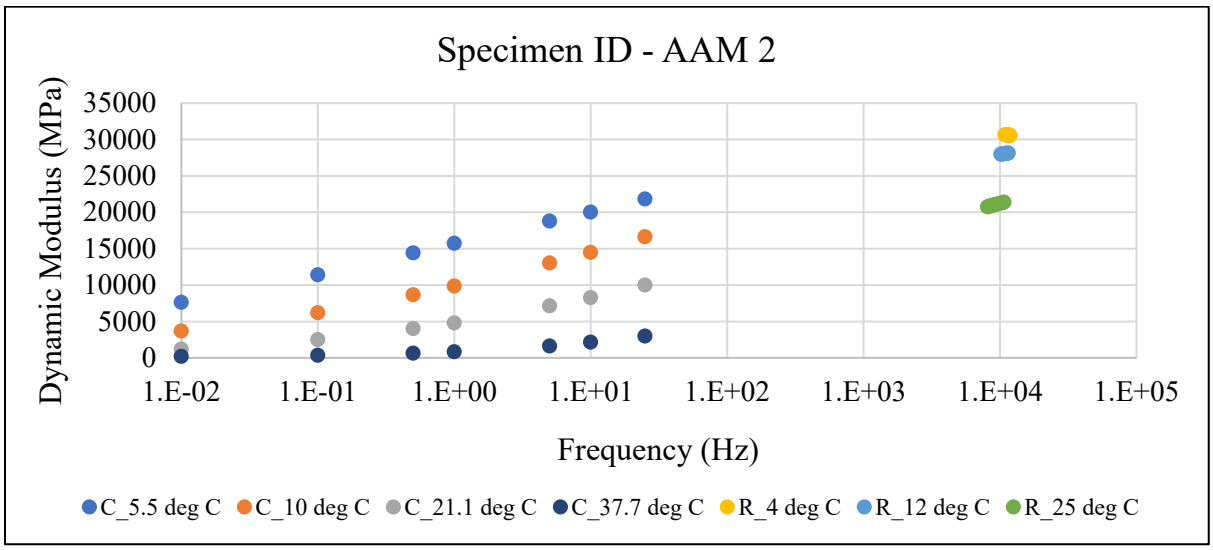

Figure 2-18 Measured Dynamic Modulus Results of the AAM 2 Mixture

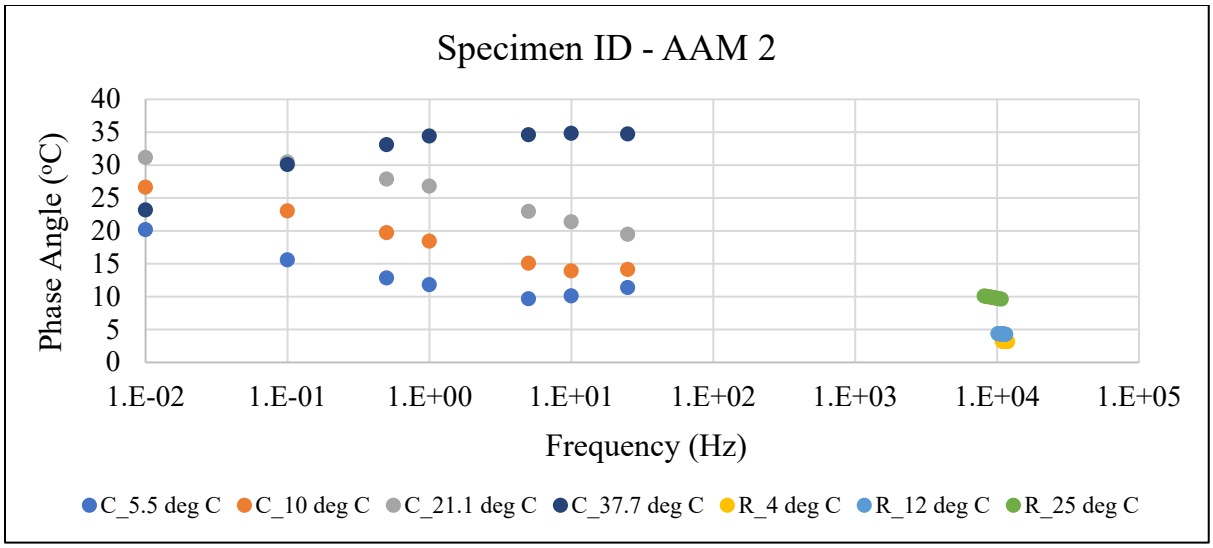

Figure 2-19 Measured Phase Angle Results of the AAM 2 Mixture

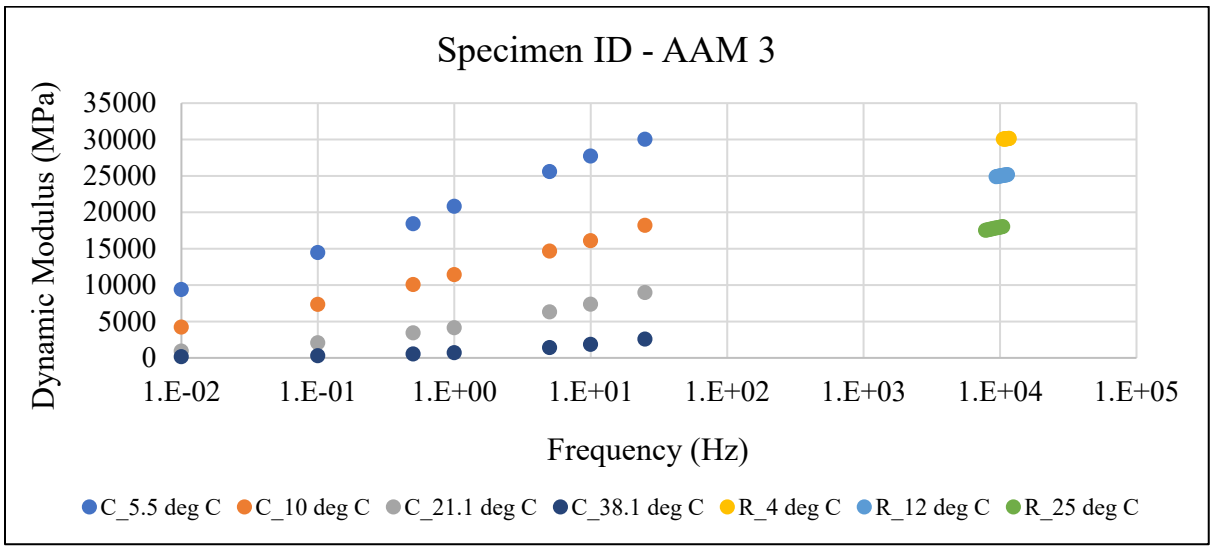

Figure 2-20 Measured Dynamic Modulus Results of the AAM 3 Mixture

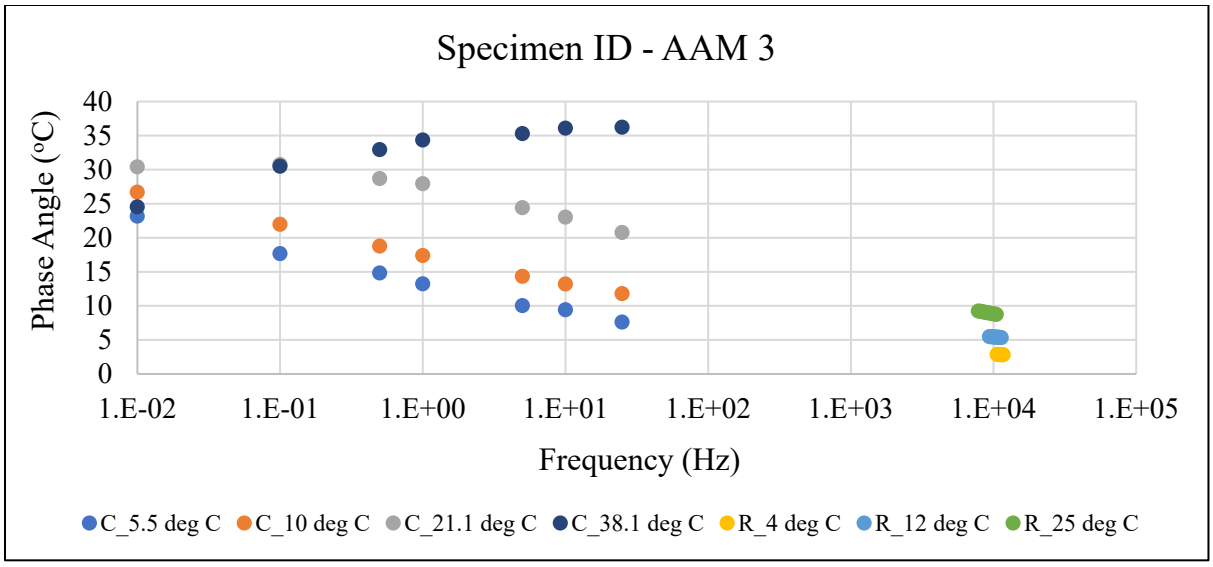

Figure 2-21 Measured Phase Angle Results of the AAM 3 Mixture

Table 2-4 Repeatability of the Two Complex Modulus Tests

	Dynamic Modulus						Phase Angle					
Specimen Type	Cyclic Test RSD%			Resonance Test RSD%			Cyclic Test RSD%			Resonance Test RSD%		
	min	max	avg	min	max	avg	min	max	avg	min	max	avg
AAD Mixtures	0.6	28.8	11.5	3.2	14.6	10.1	0	48.1	4.3	2.8	11.8	6.8
AAM Mixtures	7.6	21.6	12.7	4	8.7	6.2	0.8	24.2	5.9	7.9	20.1	13.7

Master Curve Models for Dynamic Modulus and Phase Angle

In the linear viscoelastic range, asphalt concrete can be considered as thermo-rheologically simple material (e.g., Monismith et al. 1966). Hence, time-temperature superposition is possible. Master curve construction is a technique of shifting the test data measured at various temperatures and frequencies relative to the time of loading or frequency and aligning them onto a single curve. This aids in the interpretation of asphalt behavior by extrapolating the material properties to frequencies and temperatures difficult to attain during the testing.

The first step in constructing a master curve is to choose a reference temperature to which the remaining data is horizontally shifted using a shift factor. The shift factor a_T defines the required shift at a given temperature, by which the frequency is multiplied to obtain a reduced frequency (Equation 2-5).

$$f_r = a_T * f \quad \textbf{(2-5)}$$

where f is the loading frequency at any temperature and f_r is the corresponding reduced frequency at the reference temperature.

There are several shift factors functions available in the literature like the Arrhenius equation, Williams Landel and Ferry (WLF) equation, log-linear equation, second-order polynomial equation, VTS equation, etc., suitable for asphalt binders and mixtures (Mirza and Witczak 1995, Painter and Coleman 1997, Williams et al. 1955, Yusoff et al. 2011b).

A dynamic modulus master curve is usually represented as a sigmoidal function (ARA 2004, Andrei, Witczak and Mirza, 1999, Fonseca and Witczak, 1996, Gopalakrishnan et al. 2014, Pellinen et al. 2004, Schwartz 2005, Witczak 2005). The sigmoidal coefficients and the time-temperature shift factors are solved simultaneously by using a non-linear minimization algorithm to match the sigmoidal function to the dynamic modulus data measured at different temperatures and frequencies. This can be justified based on the physical observations of an asphalt mixture behavior. The maximum stiffness of the mix, which is based on the limiting binder stiffness at cold temperatures, is approached asymptotically by the upper part of the sigmoidal function. At high temperatures and low frequency, as the aggregate influence becomes more dominant than viscous binder influence, the mix stiffness reaches a limiting equilibrium value that is dependent on the aggregate gradation. The sigmoidal function thus reasonably captures the physical behavior of the asphalt mixture stiffness over a broad temperature range.

AASHTO R 84 standard (2017) adopted the Hirsch Model developed by Christensen et al. (2003), a logistic sigmoidal function, and the Arrhenius shift factor for developing dynamic modulus master curve using the AMPT results. The following equation (2-6) presents the Hirsch model for a limiting binder modulus of 1 GPa.

$$|E^*|_{max} = P_c\left[4200000\left(1-\frac{VMA}{100}\right)+435000\left(\frac{VFA*VMA}{10000}\right)\right.$$
$$\left.+(1-P_c)*\left[\frac{\left(1-\frac{VMA}{100}\right)}{4200000}+\frac{VMA}{435000(VFA)}\right]^{-1}\right] \quad \textbf{(2-6)}$$

$$P_c = \left(20+\frac{435000(VFA)}{VMA}\right)^{0.58}*\left[650+\left(\frac{435000(VFA)}{VMA}\right)^{0.58}\right]^{-1}$$

where $|E^*|_{max}$ is the maximum limiting modulus in psi, VMA is the percent voids in mineral aggregate, and VFA is the percent voids filled with asphalt.

The Arrhenius time-temperature shift factor is presented in equation 2-7. Only one constant ΔE_a must be calculated in this expression, which defines the minimum energy required before the occurrence of intermolecular movement.

$$\log a_T = \frac{\Delta E_a}{19.14714}\left(\frac{1}{T}-\frac{1}{T_r}\right) \quad \textbf{(2-7)}$$

where ΔE_a is the activation energy (fitting parameter), T is the test temperature in K, and T_r is the reference temperature in K.

The dynamic modulus master curve equation is given in Equation 2-8.

$$\log|E^*| = \delta + \frac{(Max - \delta)}{1 + e^{\beta+\gamma*logf_r}} \quad \textbf{(2-8)}$$

where |E*| is the dynamic modulus in psi, f_r is the reduced frequency in Hz, δ, β, γ are the fitting parameters, and Max is the logarithm of limiting maximum modulus.

This method was used in the study to construct the master curves of the mixtures with the cyclic test results at a reference temperature of 20ºC. Table 2-5 presents the master curve parameters and goodness-of-fit statistics for all the mixtures. The goodness-of-fit parameters were calculated based on the formulae given in AASHTO R 84, and the normalized root mean square deviation (NRMSD) was determined based on equation 2-9.

$$NRMSD = \frac{\sqrt{\frac{\sum_{i=1}^{N}(y_{p_i} - y_i)^2}{N}}}{\max(y) - \min(y)} \quad \textbf{(2-9)}$$

where y_p is the predicted dynamic modulus in MPa, y is the measured dynamic modulus in MPa, N is the number of measurements, and i is the index of the measurement.

Table 2-5 Estimated Parameter Values of the AASHTO R 84 Model to Match Cyclic Test Measurements

Specimen ID		ΔE_a	δ	β	γ	S_e/S_y	R^2	NRMSD
All	Initial Values	200000	0.50	-1.00	-0.5			
AAD 1	Final Values	174778	4.13	-0.53	-0.63	0.17	0.974	0.035
AAD 2		188408	3.74	-0.67	-0.59	0.12	0.987	0.033
AAD 3		198360	3.80	-0.74	-0.59	0.11	0.989	0.025
AAM 1		226974	3.11	-1.45	-0.50	0.16	0.978	0.047
AAM 2		236710	3.73	-1.22	-0.54	0.16	0.978	0.051
AAM 3		240056	3.61	-1.24	-0.54	0.13	0.985	0.045

Although the curves' goodness-of-fit parameters and NRMSD were very positive, this procedure disregards the phase angle data that provides important linear viscoelastic information about the material (Yusoff et al. 2011a). The master curves produced using this method may be biased in characterizing the material's behavior, resulting in non-compliance with the linear viscoelastic theory (Zhao et al. 2013). Further, it was not possible to extend the AASHTO R 84 method for developing a master curve using the resonance test data. Hence, the Havriliak–Negami (HN) model (Equation 2-4) was later used instead of the sigmoidal function, considering the model's ability to characterize the complex modulus. The Havriliak–Negami model can account for an asymmetrical loss peak and has been shown to be very effective in modeling viscoelastic material behavior (Gudmarsson et al. 2012, Gudmarsson 2014a, Hartmann et al. 1994, Madigosky et al. 2006, Zhao et al. 2013). The WLF relationship given in equation 3-10 was used to calculate the shift factors.

$$\log(a_T) = \frac{-C_1(T - T_{ref})}{C_2 + T - T_{ref}} \quad \textbf{(2-10)}$$

where T is the test temperature, T_{ref} is the reference temperature, and C_1, C_2 are the material constants.

The estimated values of the unknown coefficients in the HN model and the WLF shift factor, along with the resulting normalized root mean square deviation, are presented in Tables 2-6 and 2-7.

Table 2-6 Estimated Parameter Values of the HN Model to Match the Cyclic Test Measurements

Specimen ID		E_∞ (MPa)	E_o (MPa)	α	β	τ	C_1	C_2	NRMSD
All	Initial Values	45000	100	0.4	0.3	0.1	12	120	
AAD 1	Final Values	45815	354	0.405	0.195	0.015	7.7	72.7	0.037
AAD 2		45517	200	0.480	0.124	0.034	7.2	66.0	0.022
AAD 3		58915	22	0.434	0.104	0.075	15.2	143.1	0.022
AAM 1		260251	568	0.345	0.026	0.245	13.5	105.8	0.048
AAM 2		94060	235	0.379	0.063	0.259	9.0	65.6	0.027
AAM 3		113848	203	0.340	0.072	0.065	11.3	70.4	0.081

Table 2-7 Estimated Parameter Values of the HN Model to Match the Resonance Test Measurements

Specimen ID		E_∞ (MPa)	E_o (MPa)	α	β	τ	C_1	C_2	NRMSD
All	Initial Values	45000	100	0.4	0.3	0.1	12	120	
AAD 1	Final Values	45000	100	0.362	0.235	0.051	12.0	119.9	0.096
AAD 2		45000	100	0.376	0.241	0.028	12.0	120.0	0.065
AAD 3		45000	100	0.421	0.156	0.076	12.1	120.0	0.181
AAM 1		45000	100	0.374	0.190	0.196	12.0	120.0	0.054
AAM 2		45000	100	0.416	0.240	0.019	12.0	120.0	0.047
AAM 3		42831	100	0.352	0.321	0.005	11.1	108.5	0.083

Initially, the measured test data were plotted in Cole-Cole space to assess the quality of the test data before using it in the analysis. If material is viscoelastic and thermo-rheologically simple, a single curve can be obtained in the Cole-Cole complex space, regardless of loading frequency or temperature (Gudmarsson et al. 2014b). Figures 2-22 (a) to (f) present the measured dynamic modulus of all the mixtures plotted in the Cole-Cole space. Based on the shape of the unique curves, the measured cyclic test results of AAD 3 and AAM 3 mixtures at low temperatures (4.4ºC ~ 5.5ºC) were excluded while constructing the master curve.

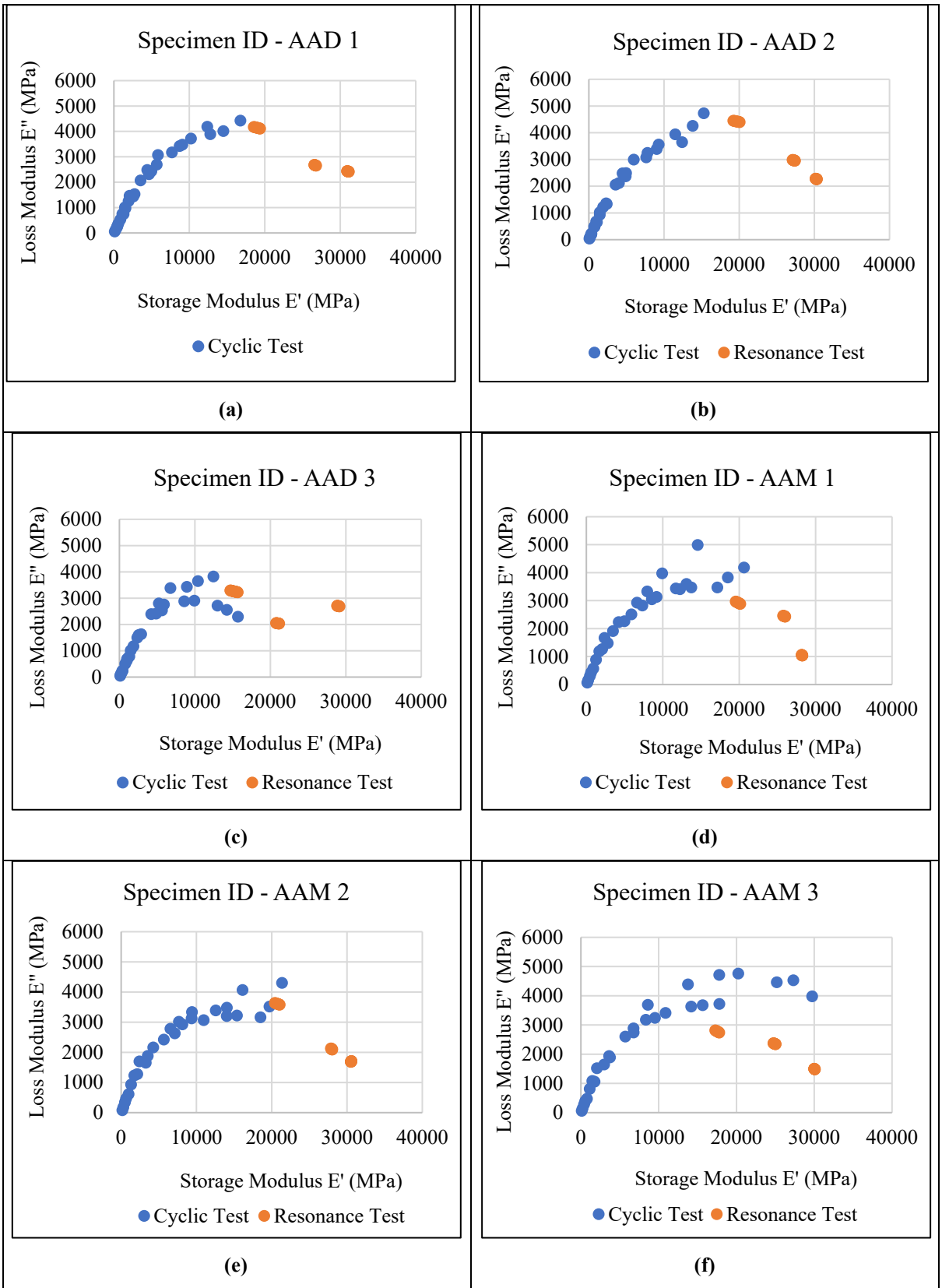

Figure 2-22 Cole-Cole Diagrams of Dynamic Moduli Determined Through Cyclic and Resonance Tests

The following section presents the master curves developed using AASHTO R 84 and HN models. The reference temperature was set as 20ºC, and the viscoelastic properties were predicted in the temperature range of -10ºC to 54.4ºC and the frequency range of 0.01 Hz to 25 Hz, as required by the AASHTO MEPDG software inputs. The master curves were constructed using the Microsoft Excel solver for the AASHTO R 84 fit model and the MATLAB non-linear least-squares optimization with the Levenberg-Marquardt algorithm for the HN model. Comparisons were made between the two models for their closeness to fit the measured cyclic test data. Further, the master curves of the mixtures developed using the HN model, and the two dynamic modulus test measurements were assessed to determine the similarity of the tests in terms of stiffness and phase angle results.

Comparisons Between the Master Curves

The master curves for all the mixtures developed using the cyclic test data are shown in Figures 2-23 (a) to (f). The measurements were fitted using the AASHTO R 84 model combined with the Arrhenius shift factor and the HN model combined with the WLF shift factor. Table 2-8 presents the normalized mean square deviation of the predicted values from the measured values. The master curve matches the absolute values of the dynamic modulus well in both models. However, the AASHTO R 84 model worked well at low to intermediate frequencies, while the HN model fitted the values well at intermediate to high frequencies.

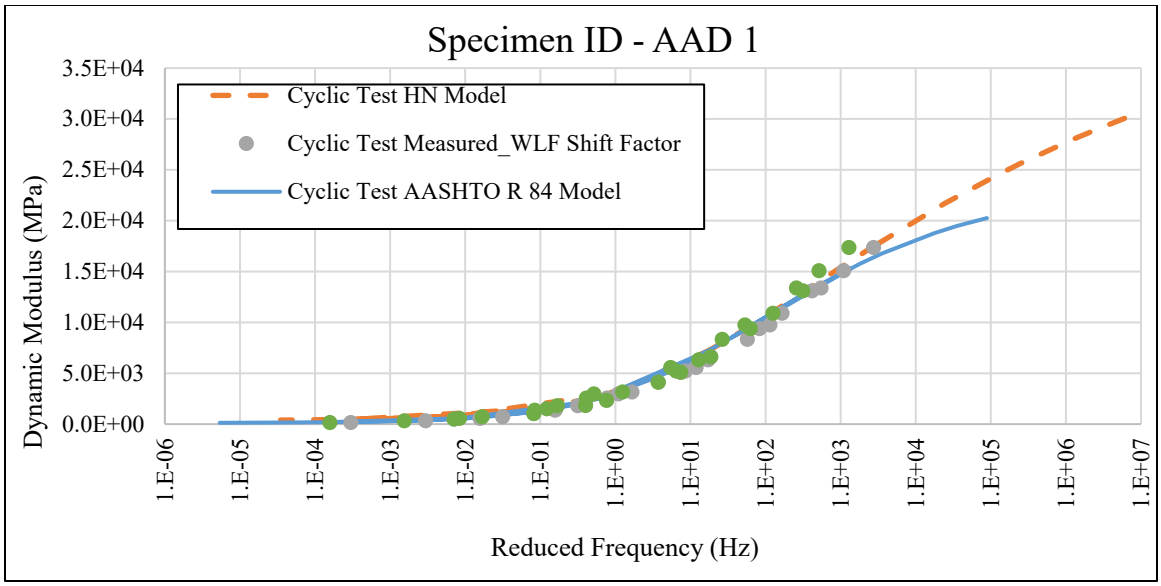

(a)

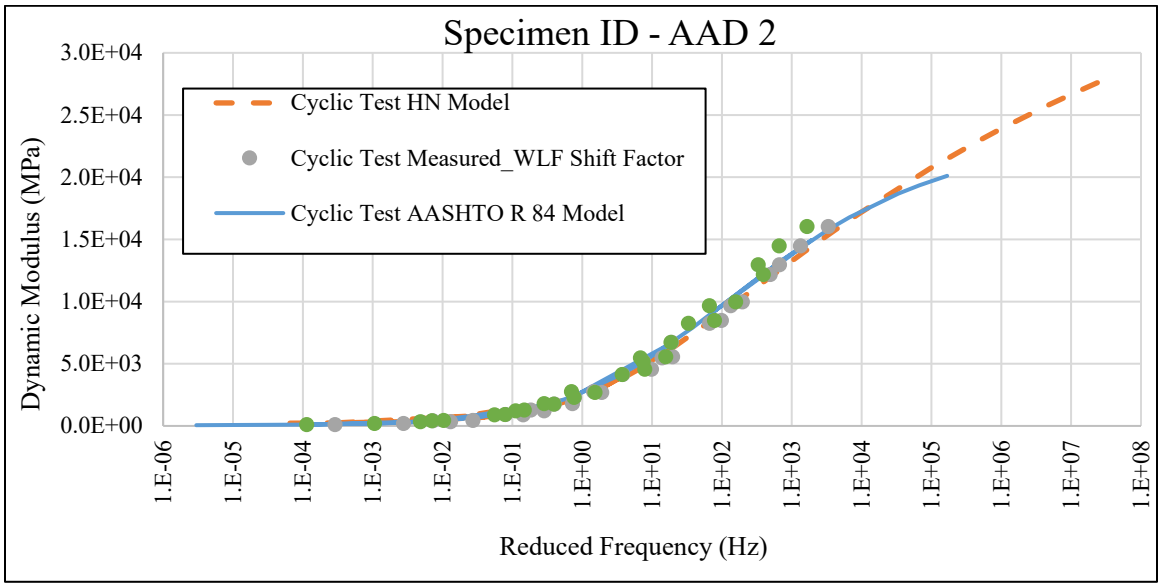

(b)

Figure 2-23 Comparison of the Cyclic Test Dynamic Modulus Master Curves at T_{ref} = 20◦C Determined Using AASHTO 84 Model and HN Model

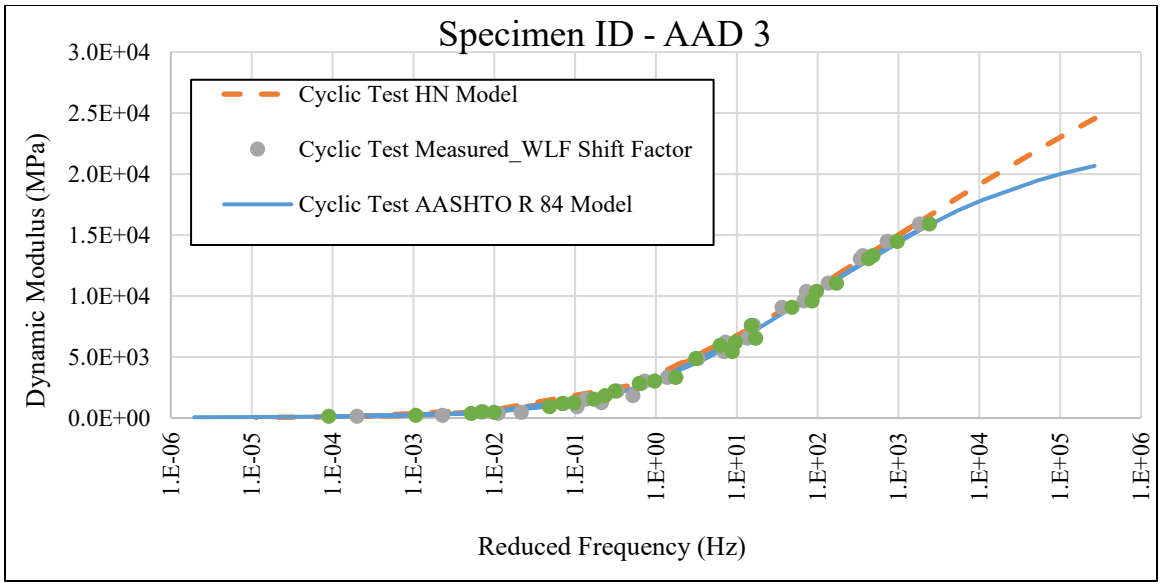

(c)

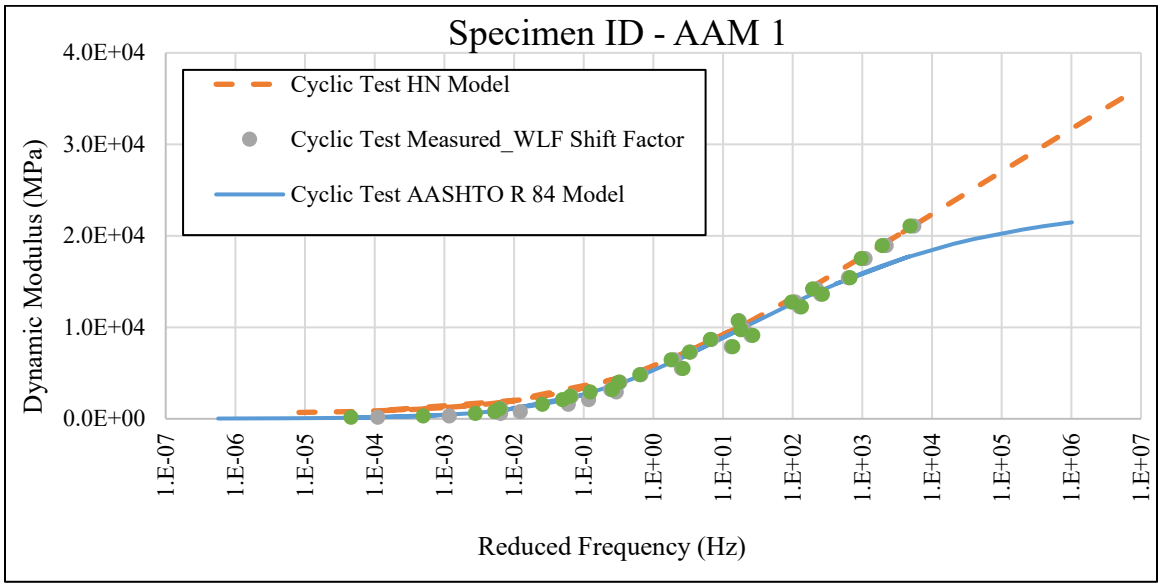

(d)

Figure 2-23 Continued

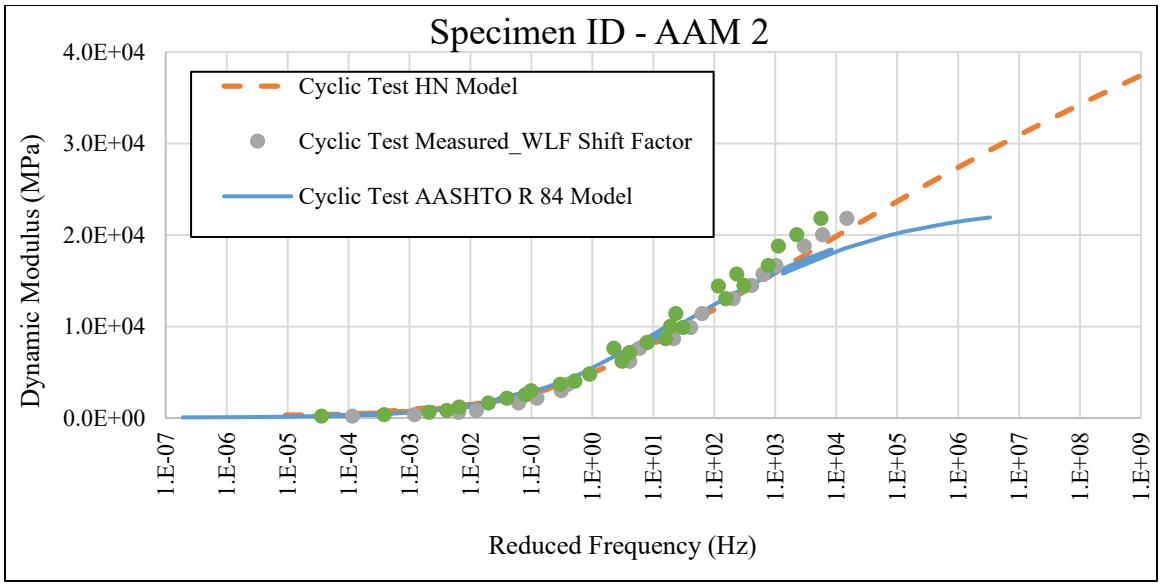

(e)

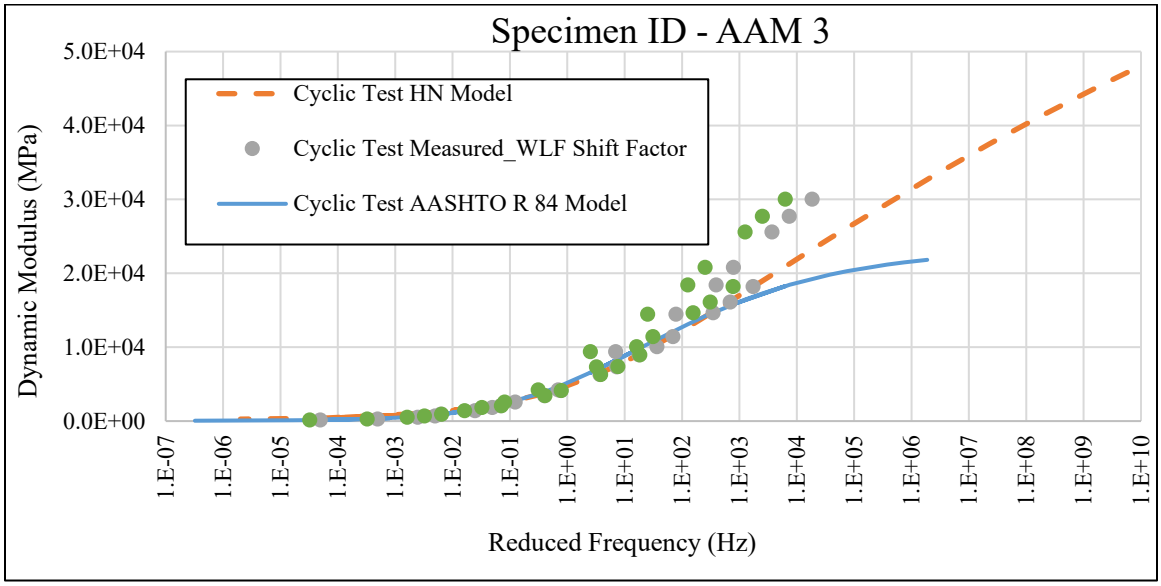

(f)

Figure 2-23 Continued

Table 2-8 Difference Between the Measured and Models Predicted Cyclic Test Dynamic Modulus

Specimen ID	Normalized Root Mean Square Deviation	
	AASHTO R 84 Model	HN Model
AAD 1	0.035	0.037
AAD 2	0.033	0.022
AAD 3	0.025	0.022
AAM 1	0.047	0.048
AAM 2	0.051	0.027
AAM 3	0.045	0.081

Figures 2-24 to 2-35 show the master curves of the dynamic modulus and the phase angle constructed using the HN model and the results from the two test methods. Table 2-9 displays the dynamic moduli ratios and the phase angle ratios for both test methods at 21.1°C (~T_{ref}) temperature condition. Based on the master curves and the ratios, for AAD mixtures, the resonance test resulted in a higher dynamic modulus and a lower phase angle than the cyclic test. The trend was opposite for the AAM mixtures, i.e., the dynamic modulus and the phase angle from the resonance test were lower and higher, respectively, when compared with the cyclic test results.

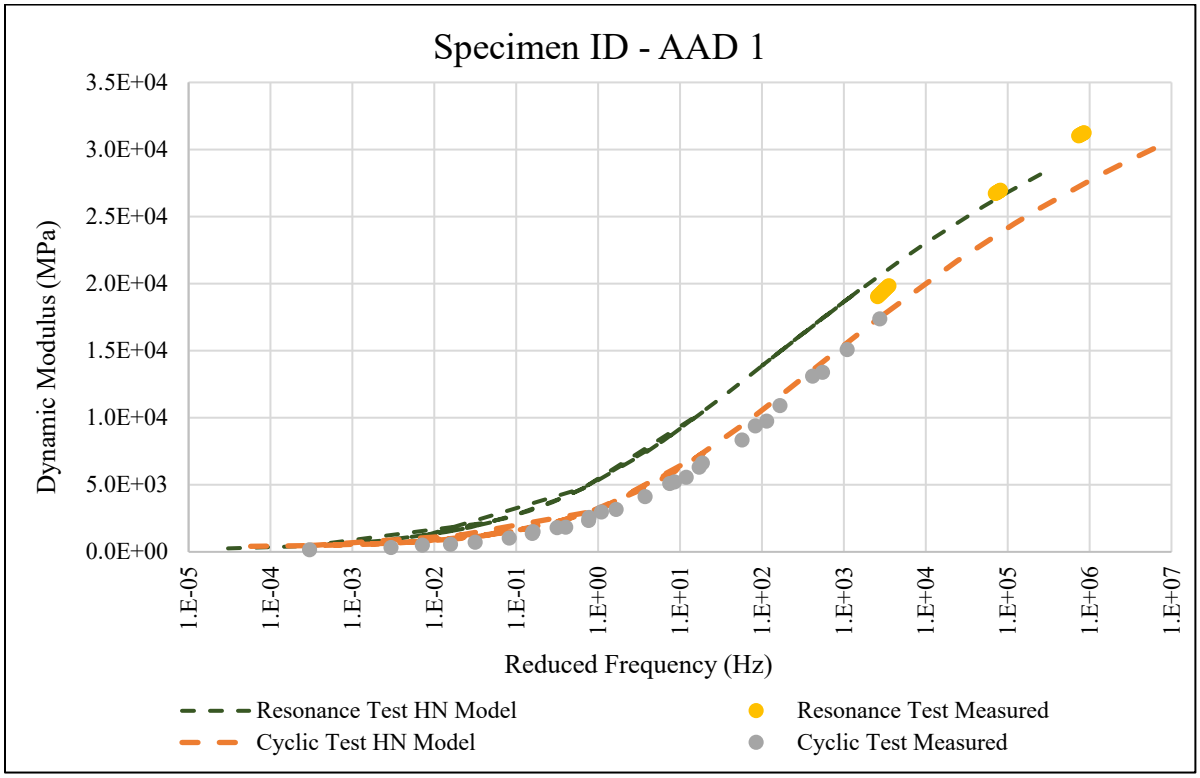

Figure 2-24 Comparison of the Dynamic Modulus of AAD 1 Mixture Determined by the Cyclic and Resonance Tests

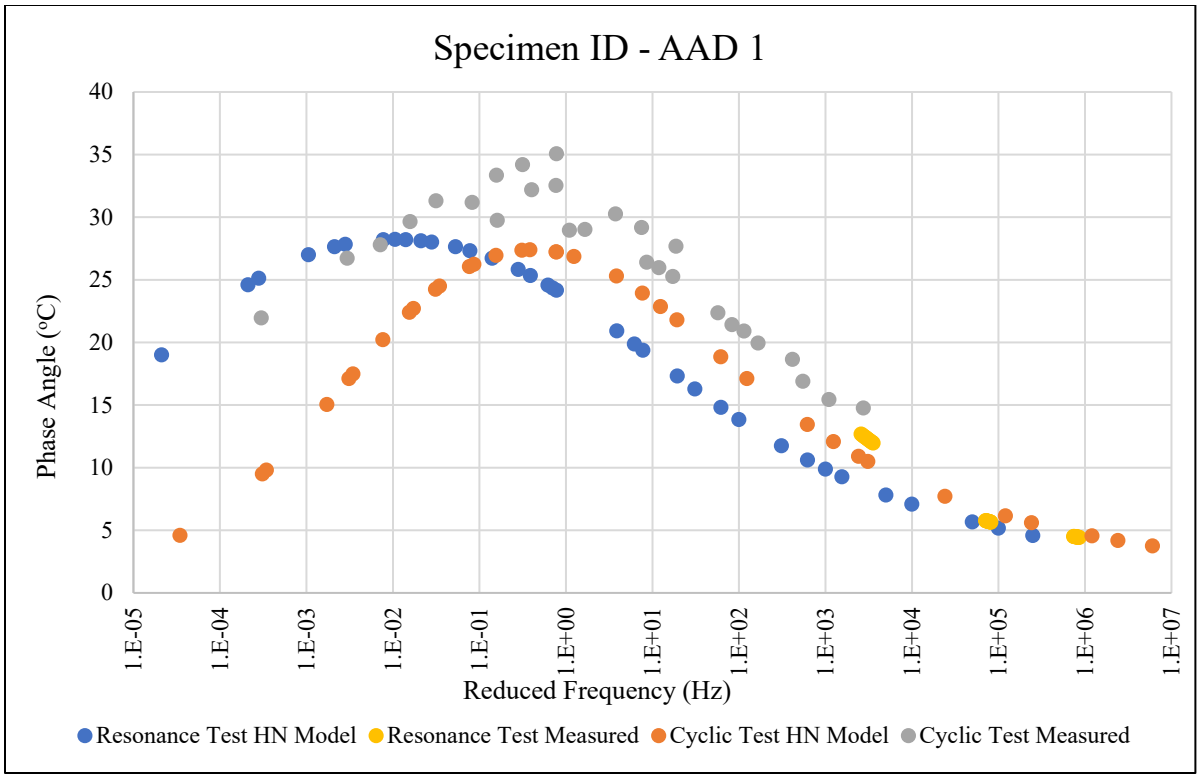

Figure 2-25 Comparison of the Phase Angle of AAD 1 Mixture Determined by the Cyclic and Resonance Tests

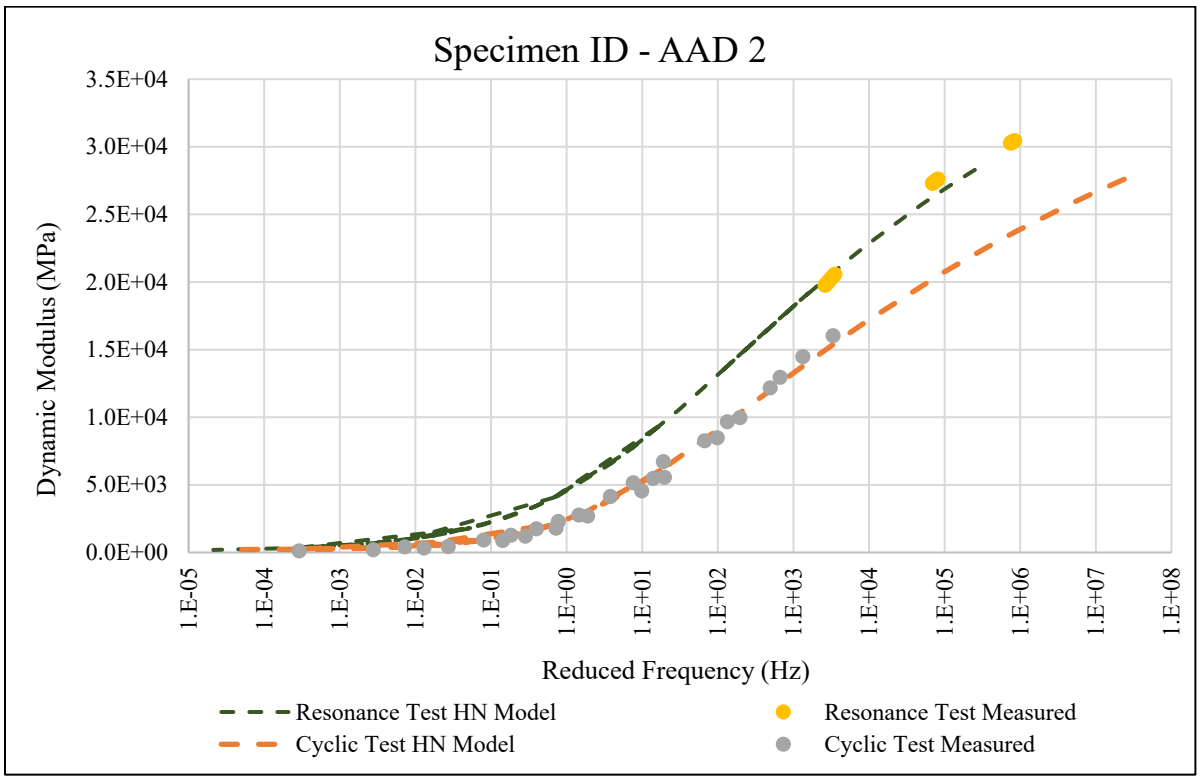

Figure 2-26 Comparison of the Dynamic Modulus of AAD 2 Mixture Determined by the Cyclic and Resonance Tests

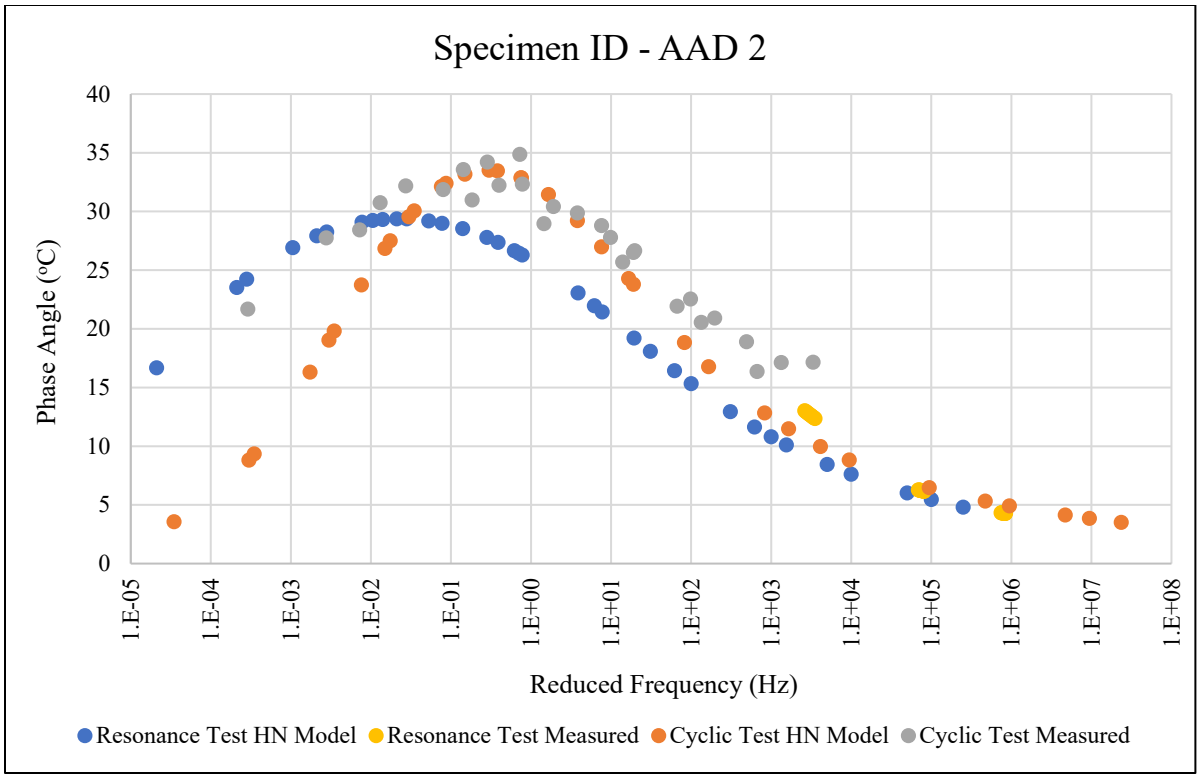

Figure 2-27 Comparison of the Phase Angle of AAD 2 Mixture Determined by the Cyclic and Resonance Tests

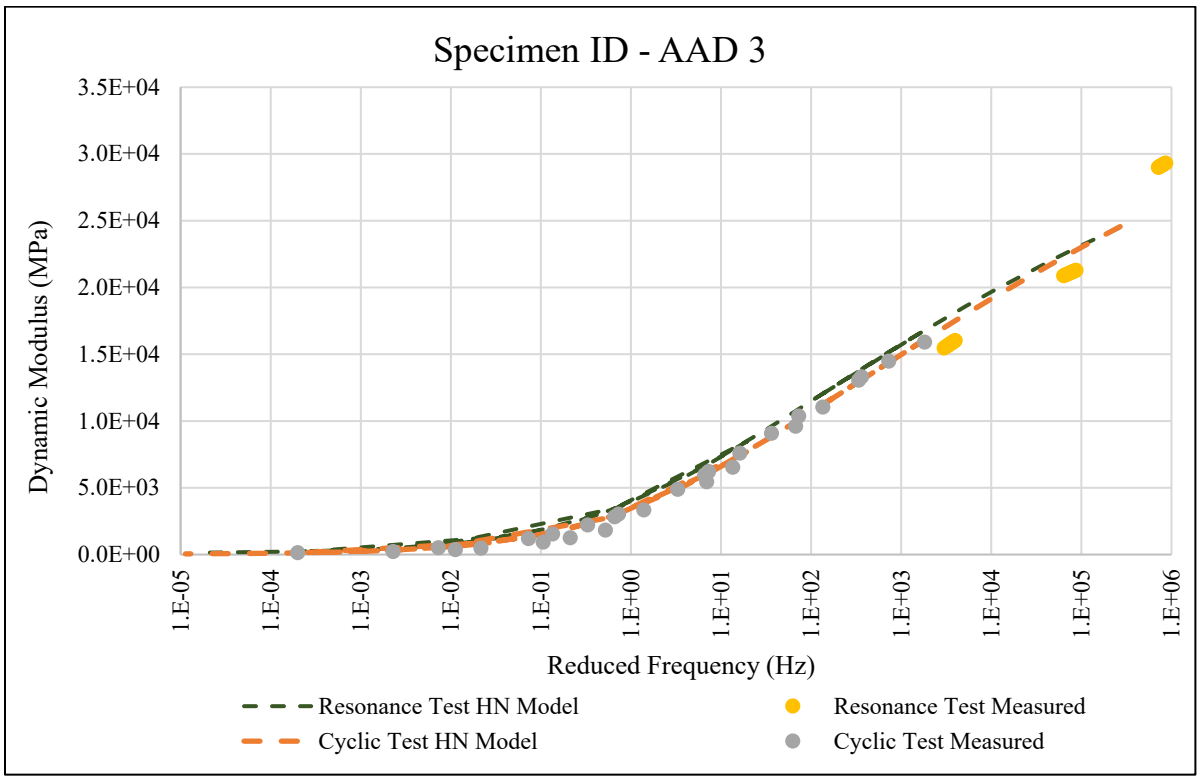

Figure 2-28 Comparison of the Dynamic Modulus of AAD 3 Mixture Determined by the Cyclic and Resonance Tests

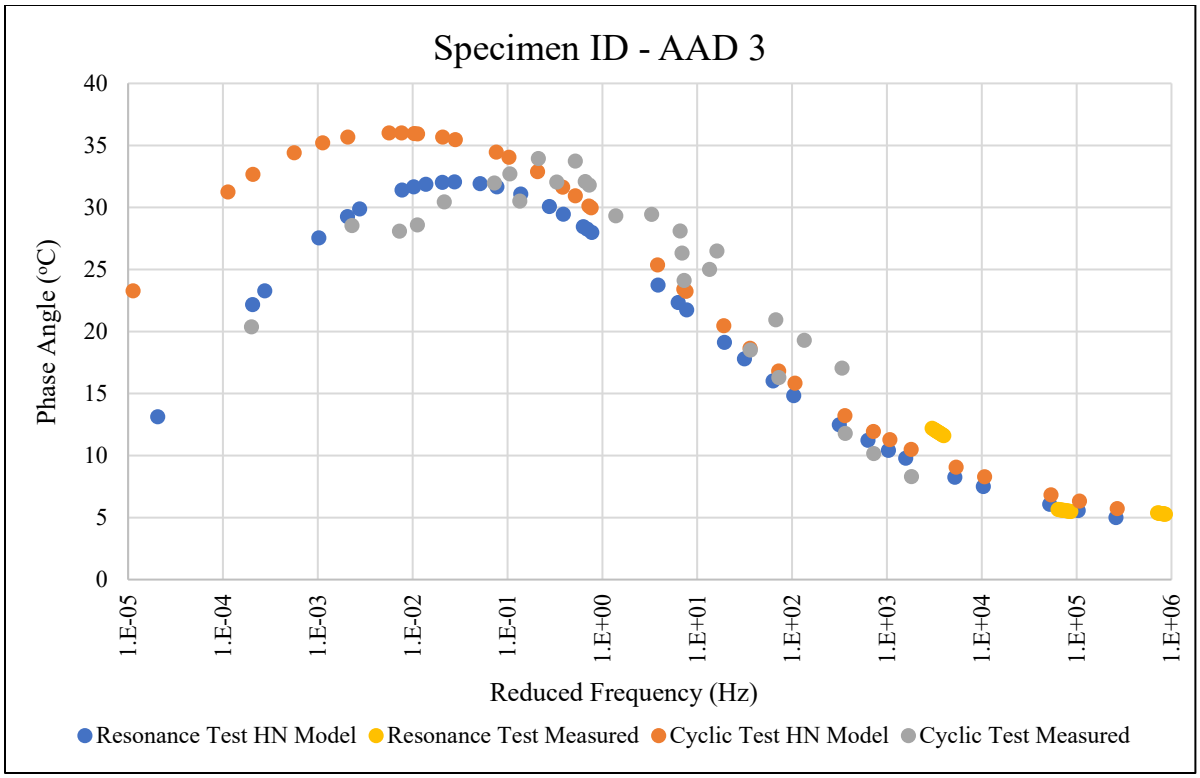

Figure 2-29 Comparison of the Phase Angle of AAD 3 Mixture Determined by the Cyclic and Resonance Tests

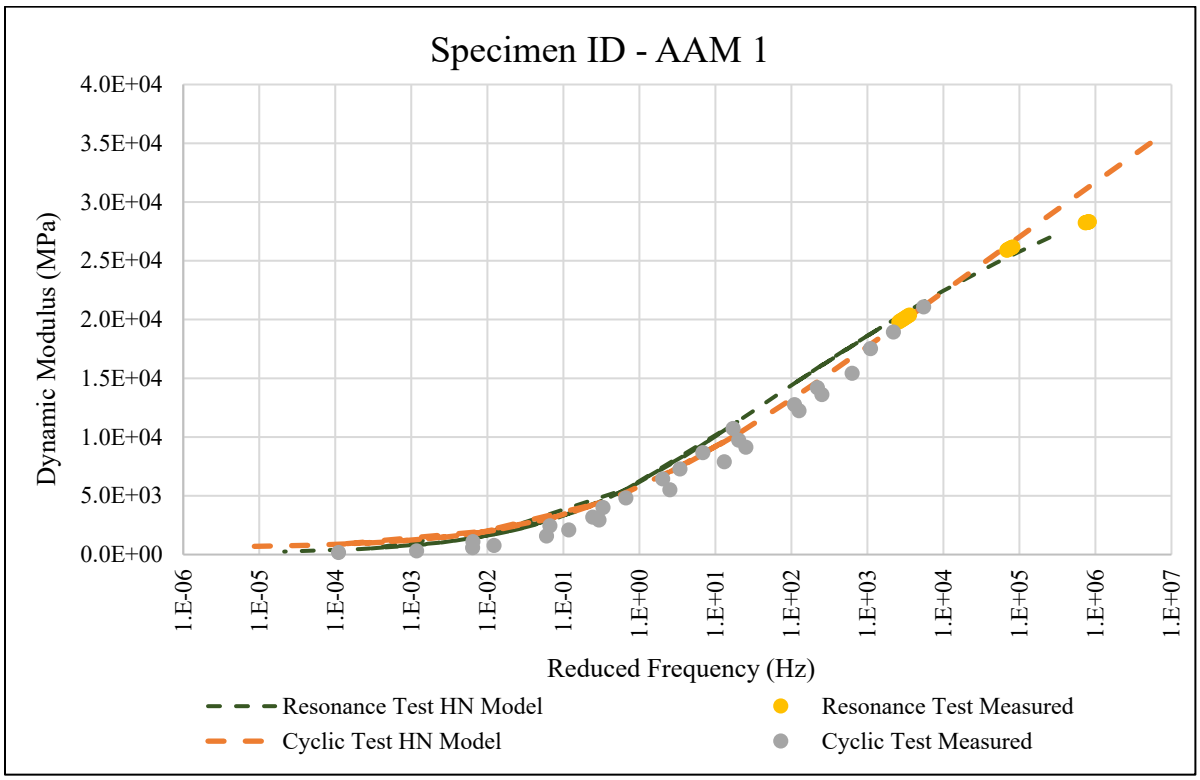

Figure 2-30 Comparison of the Dynamic Modulus of AAM 1 Mixture Determined by the Cyclic and Resonance Tests

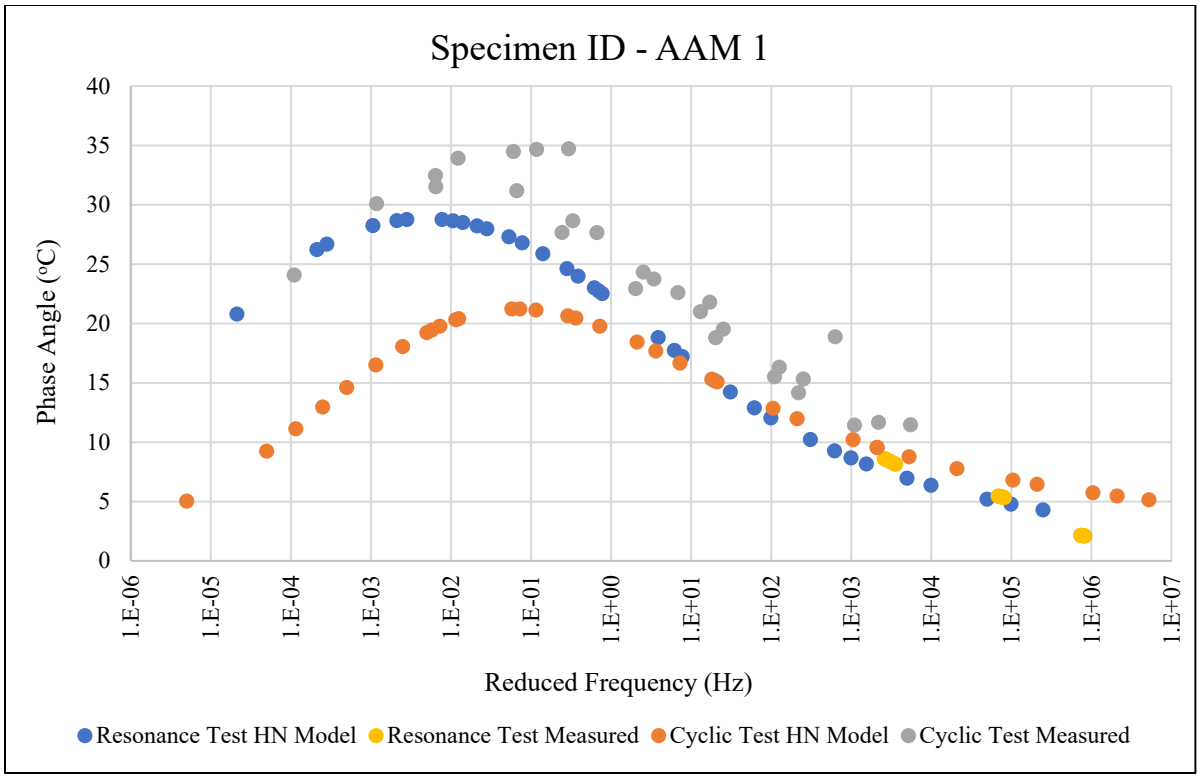

Figure 2-31 Comparison of the Phase Angle of AAM 1 Mixture Determined by the Cyclic and Resonance Tests

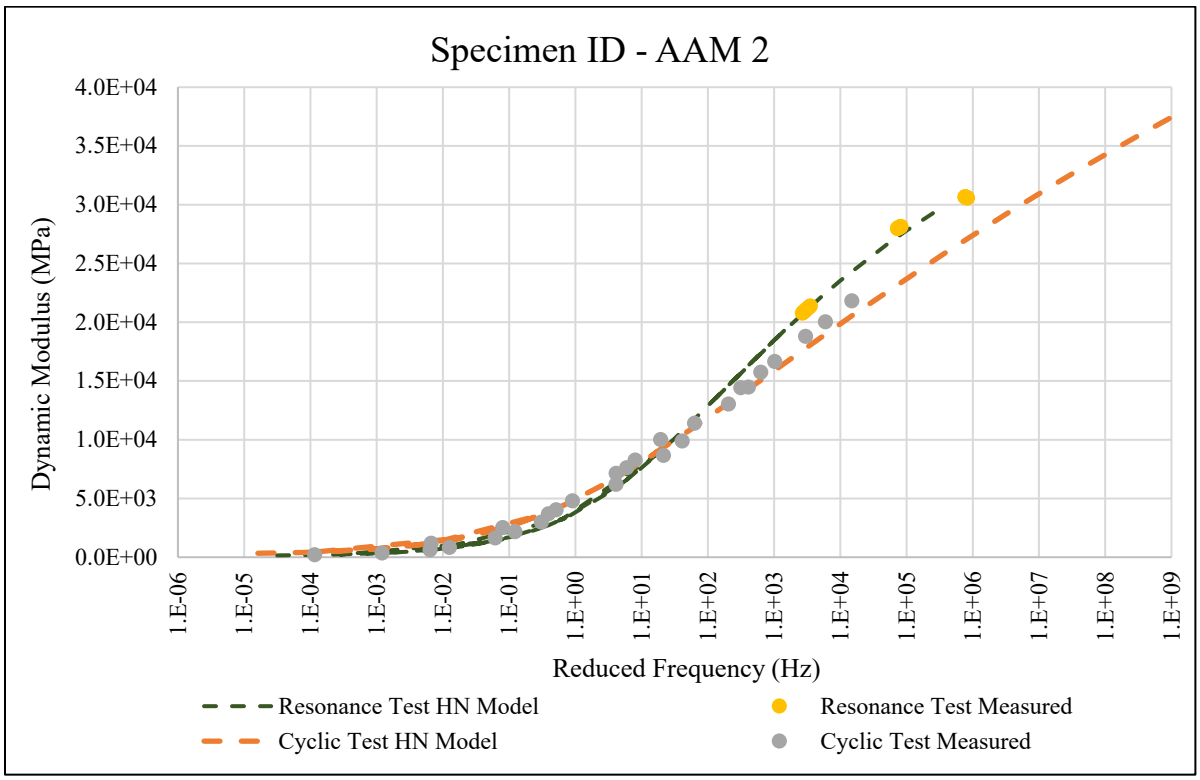

Figure 2-32 Comparison of the Dynamic Modulus of AAM 2 Mixture Determined by the Cyclic and Resonance Tests

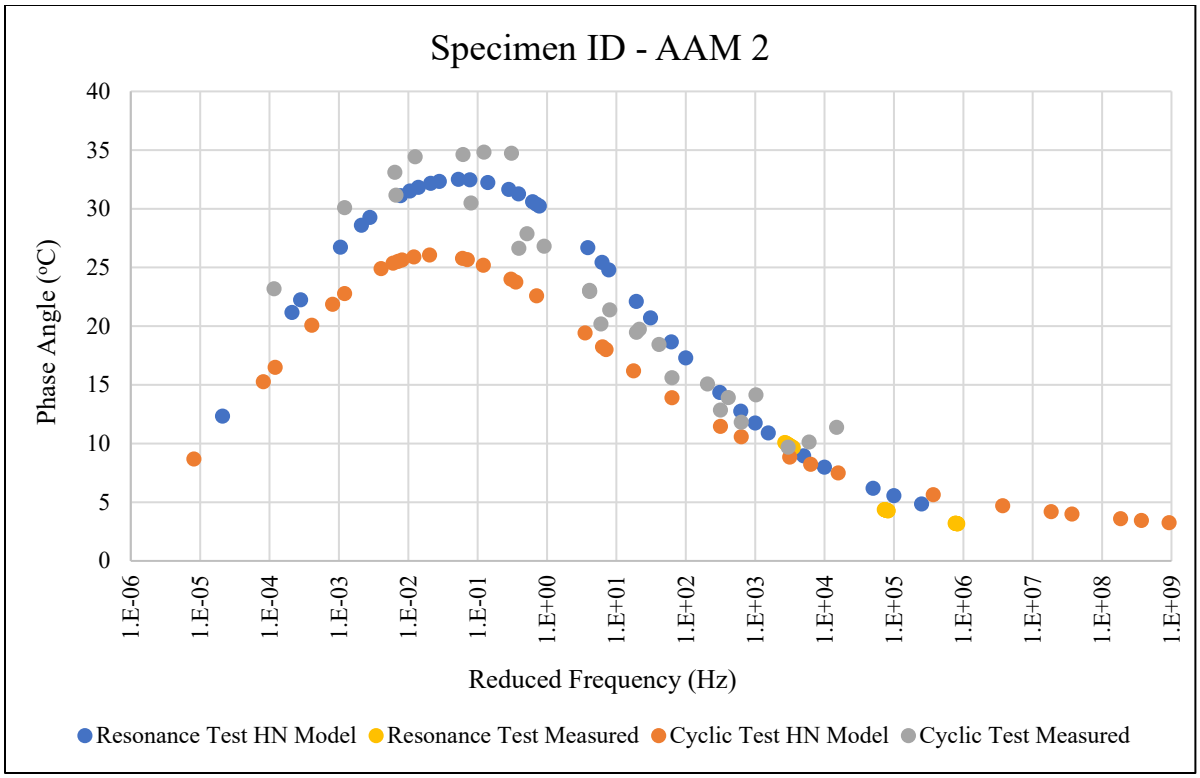

Figure 2-33 Comparison of the Phase Angle of AAM 2 Mixture Determined by the Cyclic and Resonance Tests

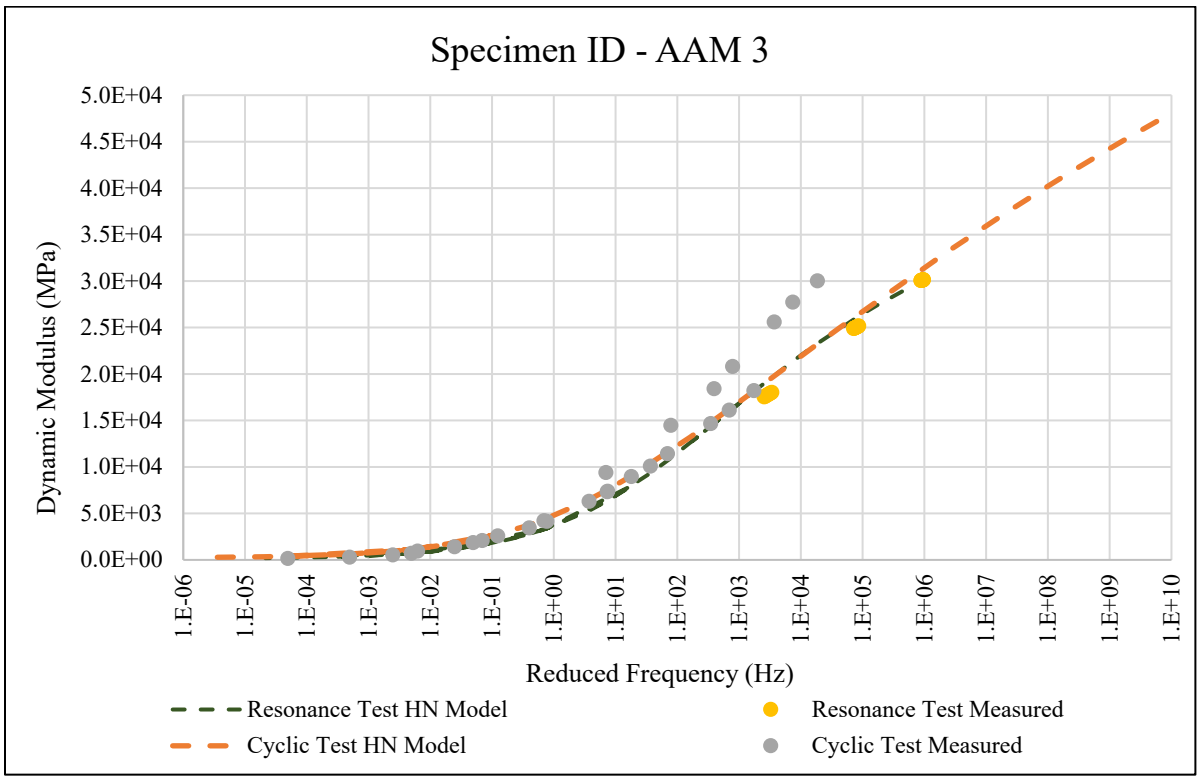

Figure 2-34 Comparison of the Dynamic Modulus of AAM 3 Mixture Determined by the Cyclic and Resonance Tests

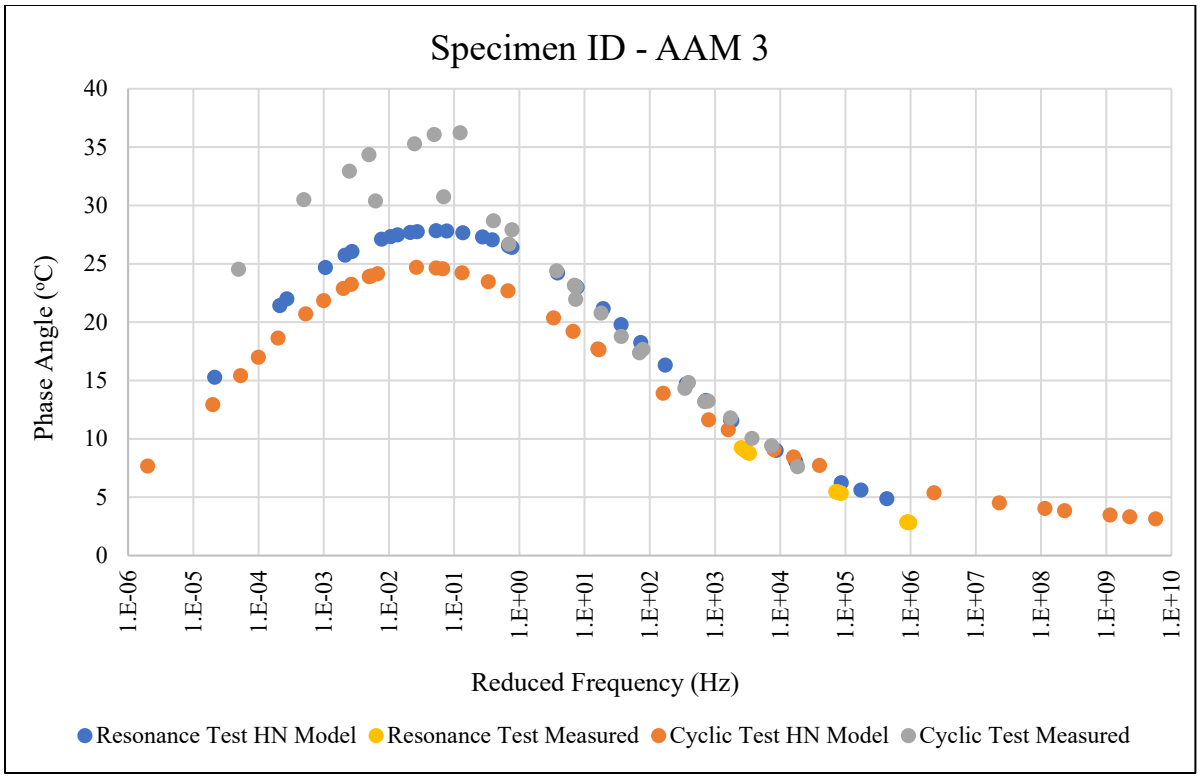

Figure 2-35 Comparison of the Phase Angle of AAM 3 Mixture Determined by the Cyclic and Resonance Tests

Table 2-9 Ratios of the Dynamic Modulus and Phase Angles at T = 21.1°C Determined Through Resonance (HN model) and Cyclic Testing (HN model)

Frequency (Hz)		25	10	5	1	0.5	0.1	0.01
$\frac{\lvert E^* \rvert_R}{\lvert E^* \rvert_C}$	AAD 1	1.43	1.50	1.55	1.68	1.72	1.75	1.57
	AAD 2	1.55	1.63	1.71	1.94	2.05	2.27	2.26
	AAD 3	1.10	1.12	1.13	1.17	1.19	1.24	1.35
	AAM 1	1.11	1.11	1.11	1.07	1.05	0.97	0.81
	AAM 2	1.00	0.94	0.89	0.77	0.72	0.64	0.54
	AAM 3	0.91	0.87	0.84	0.79	0.77	0.72	0.67
$\frac{\delta_R}{\delta_C}$	AAD 1	0.79	0.81	0.83	0.89	0.92	1.05	1.40
	AAD 2	0.81	0.79	0.79	0.80	0.82	0.90	1.23
	AAD 3	0.93	0.94	0.94	0.93	0.93	0.92	0.87
	AAM 1	0.99	1.03	1.06	1.14	1.17	1.26	1.46
	AAM 2	1.37	1.38	1.38	1.34	1.32	1.27	1.22
	AAM 3	1.20	1.20	1.19	1.16	1.15	1.13	1.12

Conclusions

Two non-destructive laboratory test methods available for determining the dynamic modulus of asphalt mixtures were investigated. One is the traditional cyclic test performed at 0.1 Hz to 25 Hz, and the other is a relatively new resonance test conducted at 8 kHz to 20 kHz frequencies. The dynamic modulus master curves with cyclic test measurements were fitted using AASHTO R 84 and HN models. Results show that the HN model overestimated the mixture stiffness at low frequencies while the AASHTO R 84 model underestimated the stiffness values at high frequencies. At intermediate frequencies, both the models gave very similar results of the dynamic modulus. Overall, the models could fit the laboratory measurements with less than 8 percent normalized root mean square deviation. However, no rational optimized fit values were found to match the resonance test results using the AASHTO R 84 method. The high-frequency measurements from the resonance test could be fitted only with a complex number model like the HN model. The comparison of the master curves generated from two test methods shows that the trend was binder dependent. However, the test methods were in reasonably good agreement. One way to improve the master curve fit further could be to solve the model coefficients and the shift factor coefficients in steps.

Additionally, the resonance test method had a lower COV% for the dynamic modulus results. Care must be taken while resonance testing for achieving repeatable phase angle measurements. In general, the resonance test model appeared to be a viable, faster, easier, and economical alternative to the cyclic test.

CHAPTER III

DEVELOPMENT OF A MICROMECHANICS BASED PERFORMANCE INDICATOR

Determination of the Performance Indicator

The effective properties of a mixture, including the effective stiffness, which is the interest of this thesis, depend on the local stress and strain fields in the mixture. These local fields' distribution is in turn influenced by the microstructure characteristics of the mixture like the volume fraction of phases, the shape and texture of inclusion, and the arrangement of constituents. All these characteristics were factored into the micromechanical framework developed recently by Onifade and Birgisson (2021) for characterizing the microstructural integrity and effective properties of multiphase particulate composites. Based on their model, the stiffness contrast between the mixture constituents had a significant effect on the integrity of a mixture. The microstructural integrity of a composite material was defined as its ability to transfer imposed load uniformly. The smaller the stiffness contrast, the more uniform was the load transfer within the mixture. This led to lower stress concentration and strain localization, thus resulting in higher integrity of the mixture.

The equations for determining the individual and composite stiffnesses were obtained from the above model, and a simple parameter termed the stiffness ratio is proposed. The ratio provides a linkage between the commonly measured mechanical property and the microstructure of the mixture. The stiffness ratio (SR) is defined as (Equation 3-1):

$$SR = \frac{E_{mix}}{E_{mastic}} \quad \textbf{(3-1)}$$

where E_{mix} is the predicted effective stiffness of the mixture, and E_{mastic} is the predicted stiffness of the mastic.

Theoretically, a low stiffness ratio indicates a stiff mixture with a hard binder that is susceptible to cracking. In contrast, a high stiffness ratio represents a soft mixture with low mastic stiffness, which is prone to rutting. Hence, depending on the need, the stiffness ratio can be used to determine the suitable mixture design.

Relating the Stiffness Ratio with Asphalt Mixture Performance

Introduction

In 1984, a new approach to design asphalt mixtures called Superior Performing Asphalt Pavements (Superpave) was initiated. It was a part of the Strategic Highway Research Program, intended to improve the performance of the pavements in the United States and make them durable, efficient, and safe. The aim of the Superpave mix design was to develop a cost-efficient mixture blend of binder and aggregate with sufficient asphalt binder, mixture volumetrics, workability, and satisfactory performance characteristics to meet the requirements of traffic, environment, structure, and reliability on the pavement.

The underlying basis for selecting an optimum mixture in the Superpave design is obtaining 4 percent design air voids at the design number of gyrations (N_{design}) (Cominsky et al. 1994). N_{design} is the estimated number of gyrations needed to produce a laboratory sample duplicating the density expected in the field based on 20-year traffic loading. Typically, the mixtures are constructed in the field at 7 percent in-place air voids, with the target to stabilize at 4 percent air voids over the pavement service life. However, an increase in the air voids has a significant adverse impact on pavement durability (Bonaquist 2016).

Hence, as an attempt to improve the pavement service life, the Joint Transportation Research Program proposed designing asphalt mixtures at 5 percent air voids and compacting them to the same density in the field without compromising on the pavement fatigue and rutting

performance (Hekmatfar et al. 2015). Three mixture designs were used, with various combinations of pavement categories, asphalt binder types, aggregate types, and aggregate gradations. The objective was to determine the optimum laboratory mixture design by modifying the aggregate gradation and number of Superpave gyrations without changing the effective binder volume (V_{be}) or the voids in mineral aggregates (VMA). Keeping V_{be} and VMA constant would enable retaining the pavement's durability as well as the permanent deformation characteristics. Further, field sections were laid with modified mixture designs to investigate their performance in the field when compacted to the laboratory design level. The data from Hekmatfar et al. (2015) was used in this paper:

a) to evaluate the relationship between the stiffness ratio and the pavement performance parameters, and
b) to establish the stiffness ratio parameter's sensitivity in capturing the effects of test conditions (temperature and frequency), compaction level, and mixture aging.

The following sections describe the mixture designs, the tests performed on the laboratory and field mixtures, and their correlation with the stiffness ratio.

Laboratory Mixture Designs

Three popularly used asphalt mixture designs from the Indiana Department of Transportation (INDOT) projects were chosen as the standard mixture designs. These designs reflected two traffic categories - Category 3 and 4, where Category 3 covered the traffic with $3*10^6$ to $10*10^6$ equivalent single axle loads (ESALs), and Category 4 represented the $10*10^6$ to $30*10^6$ ESALs vehicles. The mixtures were prepared at N_{design} of 100 and 4 percent air voids. Based on each mixture design, additional designs were prepared at lower N_{design}. These mixtures were called the re-designed mixtures, whose optimum binder content (OBC) was selected at 5 percent air voids

instead of the 4 percent standard. The aggregate proportions were adjusted to maintain the same V_{be} and VMA as the corresponding standard design along with meeting the design criteria. Table 3-1 gives an overview of the different laboratory mixture designs considered in the study. It can be seen that the mixtures are also categorized based on their nominal maximum aggregate size (NMAS), 9.5 mm and 19.0 mm. For Category 4, 9.5-mm mixtures, the gradation for 70 gyrations, 5 percent air voids design was near identical with the gradation for 100 gyrations, 4 percent air voids. Hence, the Category 4, 9.5-mm N_{70} combination was not studied further. Table 3-2 presents the gradations for the standard and the re-design mixtures. Different job-mix formulae were established because it was the gradation and aggregate properties, as well as their resistance to compaction, that regulated the air voids and binder material, not the gyratory compaction level (LEVELS 2010). Category 4, 19.0-mm, and Category 3, 9.5-mm asphalt mixtures were produced from limestone coarse aggregate, limestone and natural sand, and baghouse fines as filler. Whereas dolomite and slag coarse aggregates, dolomite and natural sands, and baghouse fines were used for Category 4, 9.5-mm mixtures. A PG 64-22 binder was used in all the mixtures. The volumetric properties of the mixtures at OBCs are presented in Tables 3-3 to 3-5.

Table 3-1 Experimental Design of Laboratory Mixtures

Pavement Category	Number of Gyrations	Target Air Voids (%)	NMAS	
			9.5-mm	19.0-mm
3	30	5	X	
	50	5	X	
	70	5	X	
	100	4	X	
4	30	5	X	X
	50	5	X	X
	70	5		X
	100	4	X	X

Table 3-2 Asphalt Mixtures Gradations and Combined Aggregate Specific Gravities

Mixture	Category 4, 19.0-mm				Category 3, 9.5-mm				Category 4, 9.5-mm		
Sieve Size, mm	N_{100}	N_{70}	N_{50}	N_{30}	N_{100}	N_{70}	N_{50}	N_{30}	N_{100}	N_{50}	N_{30}
25	100	100	100	100							
19	97.4	97.4	96.1	95.3							
12.5	86.4	86.4	79.9	75.5	100	100	100	100	100	100	100
9.5	77	77.4	68.4	62.1	97.4	97.3	95.6	95.4	95.3	94.7	94.1
6.3	59.6	60.7	55.1	51.8	75.8	76	71.6	72.6	72.8	72.2	71.4
4.75	51.2	52.7	48.6	46.8	65.4	65.7	60	61.6	61.9	61.3	60.5
2.36	36.5	38.2	37.8	39.3	33	34.7	38.1	43.7	34	38.2	42.4
1.18	22.8	23.9	23.9	25.5	19.1	20.4	24.6	29.5	20.4	24.9	29.2
0.6	14.6	15.3	15.3	16.6	12.4	12.9	16.1	19.4	12.8	16.4	19.7
0.3	8.5	8.8	8.8	9.7	7.8	7.7	9.5	11.3	7.6	9.9	11.5
0.15	5.6	5.7	5.6	6.4	4.9	4.4	5.3	6.0	4.2	5.7	6.1
0.075	4.4	4.5	4.4	5.1	4.0	3.4	4.0	4.5	3.0	4.3	4.6
G_{sb}	2.665	2.665	2.650	2.651	2.692	2.692	2.692	2.694	2.631	2.630	2.626

Table 3-3 Category 4, 19.0-mm Mixture Design Volumetrics

N_{design}	Avg. V_a, %	Avg. G_{sb}	Avg. VMA, %	Avg. VFA, %	P_{be}, %	Avg. Dust Ratio
100	4.0	2.665	13.6	70.6	4.1	1.1
70	4.9	2.665	14.5	66.3	4.1	1.1
50	4.9	2.650	14.4	66.0	4.1	1.1
30	4.9	2.651	14.9	67.2	4.3	1.2

Table 3-4 Category 3, 9.5-mm Mixture Design Volumetrics

N_{design}	Avg. V_a, %	Avg. G_{sb}	Avg. VMA, %	Avg. VFA, %	P_{be}, %	Avg. Dust Ratio
100	4.1	2.692	15.0	72.9	4.6	0.9
70	5.1	2.692	16.0	67.9	4.6	0.7
50	4.9	2.692	15.8	68.9	4.6	0.9
30	5.3	2.694	16.3	67.6	4.7	0.9

Table 3-5 Category 4, 9.5-mm Mixture Design Volumetrics

N_{design}	Avg. V_a, %	Avg. G_{sb}	Avg. VMA, %	Avg. VFA, %	P_{be}, %	Avg. Dust Ratio
100	3.8	2.631	15.0	74.9	4.8	0.6
50	4.9	2.630	16.4	70.0	5.0	0.9
30	5.0	2.626	16.4	69.6	5.0	0.9

The standard and the re-designed mixtures were compared based on their dynamic modulus values determined through AASHTO T 342 (2011) test method. The standard mixtures specimens were compacted to 7 percent air voids in compliance with the existing standards. And the specimens for the re-designed mixtures were produced at their anticipated in-service air voids, i.e., 5 percent. Though the flow number test was also performed on the mixtures, it was not included in the current analysis, hence not reported here.

Results and Discussion

The average dynamic modulus (|E*|) values of the mixtures measured at different temperatures (6ºC, 22ºC, 37ºC, and 50ºC) and 25 Hz, 10 Hz frequencies are presented in Tables 3-6 to 3-8.

Table 3-6 Average Dynamic Modulus Results of Category 4, 19.0-mm Mixtures in MPa

Test Conditions	25 Hz				10 Hz			
	N_{30}	N_{50}	N_{70}	N_{100}	N_{30}	N_{50}	N_{70}	N_{100}
6ºC	19554	20041	20145	16166	16770	18477	18277	14898
22ºC	11276	12465	12132	10088	10328	11097	11219	9207
37ºC	4157	4552	5299	3561	3236	3547	4251	2841
50ºC	1431	1743	1792	1366	1089	1299	1341	1052

Table 3-7 Average Dynamic Modulus Results of Category 3, 9.5-mm Mixtures in MPa

Test Conditions	25 Hz				10 Hz			
	N_{30}	N_{50}	N_{70}	N_{100}	N_{30}	N_{50}	N_{70}	N_{100}
6ºC	19715	19413	18226	16144	18492	17843	17543	15639
22ºC	10529	10480	9504	8351	9331	10042	8864	7628
37ºC	2756	2678	2529	3046	2191	2136	2092	2461
50ºC	919	1114	1081	944	671	811	789	707

Table 3-8 Average Dynamic Modulus Results of Category 4, 9.5-mm Mixtures in MPa

Test Conditions	25 Hz			10 Hz		
	N_{30}	N_{50}	N_{100}	N_{30}	N_{50}	N_{100}
6ºC	17682	17610	15632	16107	16055	14591
22ºC	8392	8308	8025	6957	6897	7364
37ºC	2970	3297	2721	2334	2632	2105
50ºC	1093	1171	971	910	829	731

Based on the dynamic modulus and flow number results, polynomial fits were established for both 10 Hz and 25 Hz data, and the optimum number of gyrations were estimated as 53, 52, and 42 gyrations for Category 4, 19-mm, Category 3, 9.5-mm, and Category 3, 9.5-mm mixtures, respectively.

Field Trials

The re-designed mixtures were placed on the field at two sections in Indiana. The first trial was an asphalt surface overlay of Category 4, 9.5-mm mixture on the State Road 13 (SR-13), and the second was a 3-inch intermediate asphalt layer of Category 3, 19.0-mm mixture on Georgetown Road.

After rigorous pre-field trial laboratory testing, two sections were built on SR-13 simultaneously, one with N_{100} standard mixture design and the other with N_{50} re-designed mixture. The optimum asphalt binder contents were selected at 4 percent air voids for the standard mixture and at 5 percent air voids for the re-designed mixture. The design VMA was found as 15.3 percent. Both original and re-designed mixtures consisted of steel slag and limestone coarse aggregates, limestone and natural sands, recycled asphalt shingles (RAS), and a PG 70-22 binder. The loose mixture samples required for testing were collected during the construction, and a portion of the

samples was conditioned according to AASHTO R 30 (2002) to simulate eight years of in-service aging.

In the Georgetown project, the standard mixture was designed using 100 gyrations and choosing the OBC at 4 percent air voids. While the re-designed mixture was designed using 30 gyrations and OBC obtained at 5 percent air voids. Both mixtures made use of limestone coarse aggregate, dolomite sand, Reclaimed Asphalt Pavement, RAS, and a PG 64-22 binder. The samples were obtained in two ways at this location. Initially, loose mixtures were collected from the trucks before leaving the hot mix plant. Later, 20 cores each of standard and re-designed mixtures were taken from the pavement immediately after construction. From the limited volumetric information reported, the VMA of the mixtures was assumed as 14.3 percent for the plant mixed laboratory compacted samples, and 15.1 percent for the plant mixed field compacted cores.

Except for the field cores, specimens were prepared in the laboratory with all the samples obtained. The field-sampled mixtures were re-heated at the lowest temperature possible, separated into suitable sizes, and compacted to make the specimens for testing. As mentioned before, according to the existing test method standards, the specimens for the standard mixture design were fabricated at 7 percent air voids. The specimens for the re-designed mixtures were produced at 5 percent air voids. Figure 3-1 depicts a schematic of all the field mixtures studied by Hekmatfar et al. (2015).

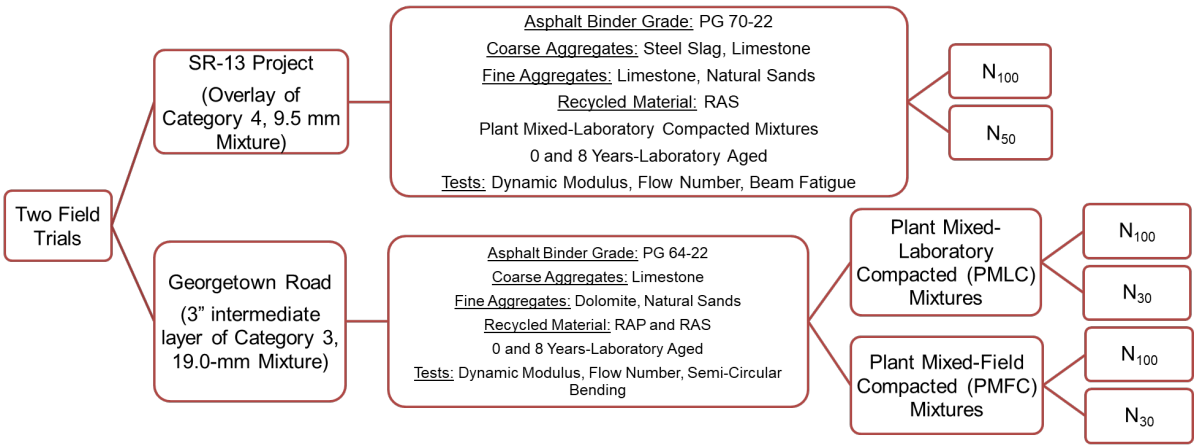

Figure 3-1 Experimental Design of Field Mixtures

Post-Field Trial Testing

The key motive for changing the mixture design method was to produce a densified asphalt layer in the field without extra compaction effort. Theoretically, additional densification would increase the pavement's resistance to rutting, and lowering the air voids slows down the oxidative aging process, thus increasing the fatigue life. These hypotheses were tested in the laboratory by conducting the dynamic modulus test and flow number test for evaluating the rutting potential, and the semi-circular bending test and beam fatigue test to assess the fatigue resistance of the mixtures.

Dynamic Modulus and Flow Number Tests:

The dynamic modulus test was performed according to AASHTO TP 79 (2013) at test temperatures ranging from 4°C to 50°C and frequencies of 0.1 Hz to 25 Hz. The more the dynamic modulus at a given temperature and frequency, the stiffer the mixture is. The unconfined flow number test was also conducted using the same equipment as the dynamic modulus (AMPT) but with deviator stress of 600 kPa applied with 0.1 sec loading time and 0.9 sec resting time, according to AASHTO TP 79. The test temperature was selected as 50.5°C, and the contact stresses were set

as 30 kPa. The concept was to measure the accumulated permanent axial strains as a function of loading cycles, and the point where the mixture exhibits tertiary flow was referred to as the flow number (FN). The flow number has a direct correlation with the rutting resistance of a mixture (Witczak 2002). A higher FN value indicates that the mixture can withstand more loading before the initiation of rutting.

Beam Fatigue Test:

The beam fatigue test was carried out at 20^{o}C according to AASHTO T 321 (2014). It was performed by repeatedly loading a beam specimen with a four-point load at a given strain level. The beam was held in place by four clamps during the procedure, and the two inner clamps were subjected to a repeated haversine load, with the outer clamps supplying a reaction load. The arrangement provided a constant bending moment at the beam's center leading to deflection measured at the center of the beam. The initial stiffness and the number of loading cycles to failure are then used to estimate the fatigue life of an asphalt mixture. Higher initial stiffness and fatigue life are favored in general.

However, it was reported that during the study, issues were faced with the temperature regulation leading to abnormal flexural stiffness values. Also, counterintuitive fatigue life results were obtained upon laboratory aging, questioning the results of the test.

Semi-Circular Bending Test:

To obtain a reliable characterization of the mixtures' fatigue behavior, the semi-circular bending test was conducted at intermediate temperature (~20^{o}C) on the Georgetown Road trial specimen following AASHTO TP 124 (2018). The test uses the elastic-plastic mechanism concept to determine the critical strain energy release rate (J_C). J_C represents the strain energy consumed to produce a unit area of the fractured surface in a mixture. It is a function of the rate of strain

energy change per notch depth. A mixture's resistance to cracking and crack propagation increases as the J_C value increases.

Results and Discussion

The consolidated results of the tests conducted on the post-field trial mixtures, obtained from two locations, are presented in the following tables 3-9 to 3-11.

Overall, testing the re-heated plant-produced mixtures yielded mixed results. Based on the dynamic modulus and flow number values, the standard design performed either better or statistically similar to the re-designed mixtures at both aging conditions. The condition of cracking performance improved slightly with the modified mixture design, which still shows potential for the re-designed mixtures to age slower in the field, resulting in the better mixture and pavement durability. The binder extracted from both the mixtures also indicate that the asphalt binder from the re-designed mixtures aged less.

Table 3-9 Summary of SR-13 Plant Mixed Laboratory Compacted Mixtures Tests Results

Test Conditions			Unaged		Aged	
Frequency (Hz)	Temperature (°C)	Test Parameter	N_{100}	N_{50}	N_{100}	N_{50}
25	4	Dynamic Modulus |E*|, GPa	19.98	16.75	21.48	20.26
25	21		11.82	9.60	14.09	13.06
25	37		6.57	4.87	8.65	8.01
25	50		3.06	2.34	5.13	4.56
10	4		18.65	15.71	20.26	19.10
10	21		10.76	8.54	12.80	11.92
10	37		5.68	4.24	7.72	7.02
10	50		2.67	1.98	4.25	3.68
10	50.5	Flow Number	6854	1899	8850	9026
10	20	Beam Fatigue, Initial Stiffness (MPa)	6572	7970	7511	8036
10	20	Beam Fatigue, Number of Cycles to Failure	604000	384000	779000	441000

Table 3-10 Summary of Georgetown Road Plant Mixed Laboratory Compacted Mixtures Tests Results

Test Conditions			Unaged		Aged	
Frequency (Hz)	Temperature (°C)	Test Parameter	N_{100}	N_{50}	N_{100}	N_{50}
25	4	Dynamic Modulus |E*|, GPa	18.24	20.33	19.78	20.60
25	21		11.49	12.33	13.13	13.28
25	37		6.21	7.13	7.67	8.28
25	50		2.77	2.78	4.36	4.07
10	4		17.42	18.79	18.42	19.40
10	21		10.83	11.59	11.77	12.30
10	37		5.53	6.13	6.78	7.21
10	50		2.29	2.19	3.63	3.36
10	50.5	Flow Number	4335	2600	8720	6001
10	20	Critical Strain Energy Release Rate J_C, J/m^2	0.860	1.402	0.776	0.747

Table 3-11 Summary of Georgetown Road Plant Mixed Field Compacted Mixtures Tests Results

Test Conditions			Unaged		Aged	
Frequency (Hz)	Temperature (°C)	Test Parameter	N_{100}	N_{50}	N_{100}	N_{50}
25	4	Dynamic Modulus |E*|, GPa	18.24	20.33	19.78	20.60
25	21		11.49	12.33	13.13	13.28
25	37		6.21	7.13	7.67	8.28
10	4		17.42	18.79	18.42	19.40
10	21		10.83	11.59	11.77	12.30
10	37		5.53	6.13	6.78	7.21
10	20	Critical Strain Energy Release Rate J_C, J/m^2	1.627	1.424	0.624	1.103

Micromechanical Model Analysis

Using the volumetrics and the dynamic modulus results from the previous sections, the stiffnesses of the individual components (aggregate and mastic) and the stiffness ratio were calculated for all standard and re-designed mixtures. Here, the binder and the fine portion of the aggregates with below 2.36 mm size were considered as the mastic. Based on the aggregate gradation and the specific gravity information, the volume fraction of aggregates (V_s) and the volume fraction of mastic (V_m) were calculated for all the mixtures. These calculated volume

fractions of the aggregate and the mastic, the measured air voids (V_a%), and the dynamic modulus of the mixture were inputted in a MATLAB optimization code for back-calculation of the stiffness of aggregate ($E_{aggregate}$) and the stiffness of mastic (E_{mastic}) at each temperature and frequency. For simplicity, the Poisson's ratios of the aggregate, the mastic, and the mixture were assumed as 0.35 across different temperatures. The start values of the E_{mastic} and $E_{aggregate}$ were taken as $\frac{E_{mix}}{2}$ GPa and 35 GPa, respectively. Although the absolute magnitudes of the stiffnesses are dependent on the initial values, it is not a concern for qualitative or relative comparison. The back-calculated moduli are inputted into a forward micromechanics model framework, where the stiffness of the mixture was predicted using the homogenization algorithm and verified with the measured stiffness. It was observed that the model was able to match exact measured stiffness at all test conditions. Finally, the ratios of mixture stiffness to mastic stiffness (E_{mix}/E_{mastic}) were determined, which are used in the following sections for characterizing the mixtures.

Laboratory Mixtures

Figures 3-2 to 3-4 present the change of individual and mixture stiffnesses along with the temperature. Because of the viscoelastic nature of an asphalt binder, the modulus of the mixture and the mastic decreases with the increase of temperature. It was interesting to observe the decrease in the slope at 37.8°C for all three mixture designs. This could indicate the point where the mastic is no more contributing to the load distribution. In asphalt mixtures, both aggregate and mastic carry the applied load up to a certain temperature. As the temperature increases, the modulus of the mastic drops due to increasing in the flow of the binder (viscous nature), and the load is primarily transferred through the aggregates. The modulus of the solids remained nearly constant at all temperatures supporting the elastic nature of the aggregates. However, this led to increased stiffness contrast between the aggregates and mastic, showing the disintegrity of the mixture.

Further, the model parameter was able to capture the change of homogeneity of the mixtures with the different number of gyrations. Though no uniform ranking of standard and re-designed mixtures that is valid at all temperatures was possible based on the stiffness ratio, the graphs suggest that overall, 70 gyrations would be optimum for Category 4, 19.0-mm mixtures, while 30 gyrations would work best for Category 3, 9.5-mm, and Category 4, 9.5-mm mixtures when permanent deformation is the primary concern. The relationship between the stiffness ratio and permanent deformation is explained in the next section.

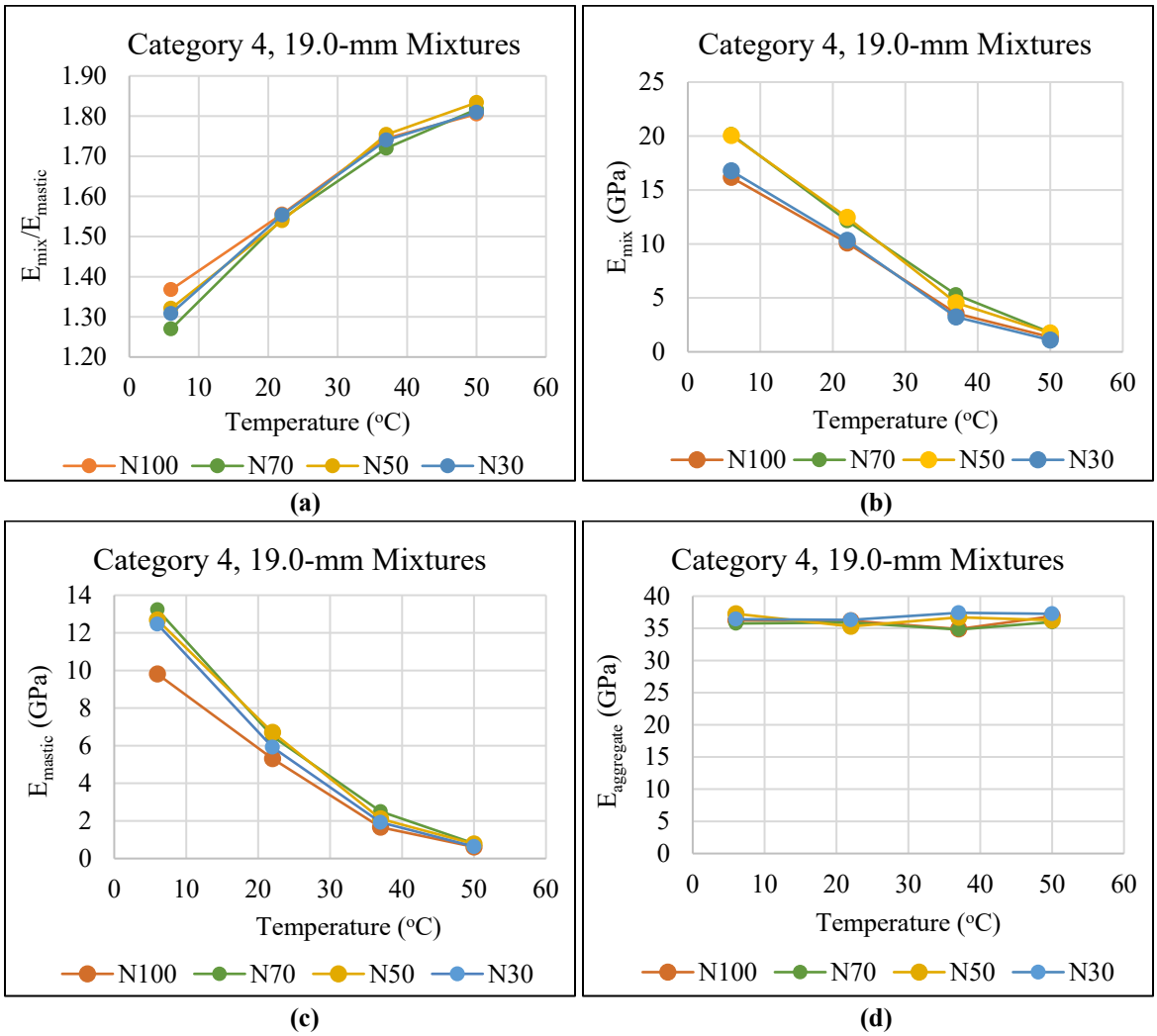

Figure 3-2 (a) Stiffness Ratio vs. Temperature for Category 4, 19.0-mm Mixtures, (b) Dynamic Modulus vs. Temperature, (c) Mastic Stiffness vs. Temperature, (d) Aggregate Stiffness vs. Temperature

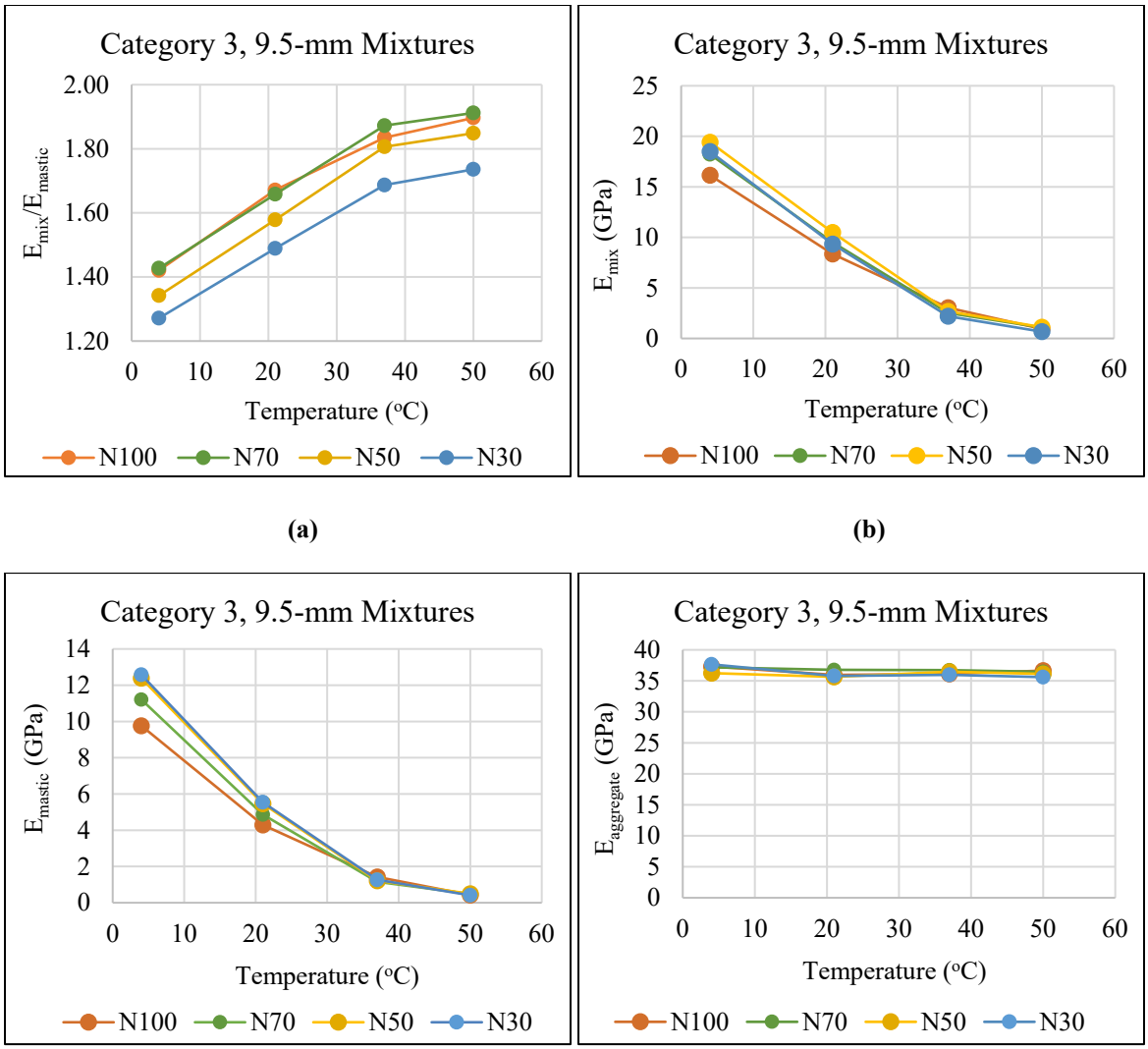

Figure 3-3 (a) Stiffness Ratio vs. Temperature for Category 3, 9.5-mm Mixtures, (b) Dynamic Modulus vs. Temperature, (c) Mastic Stiffness vs. Temperature, (d) Aggregate Stiffness vs. Temperature

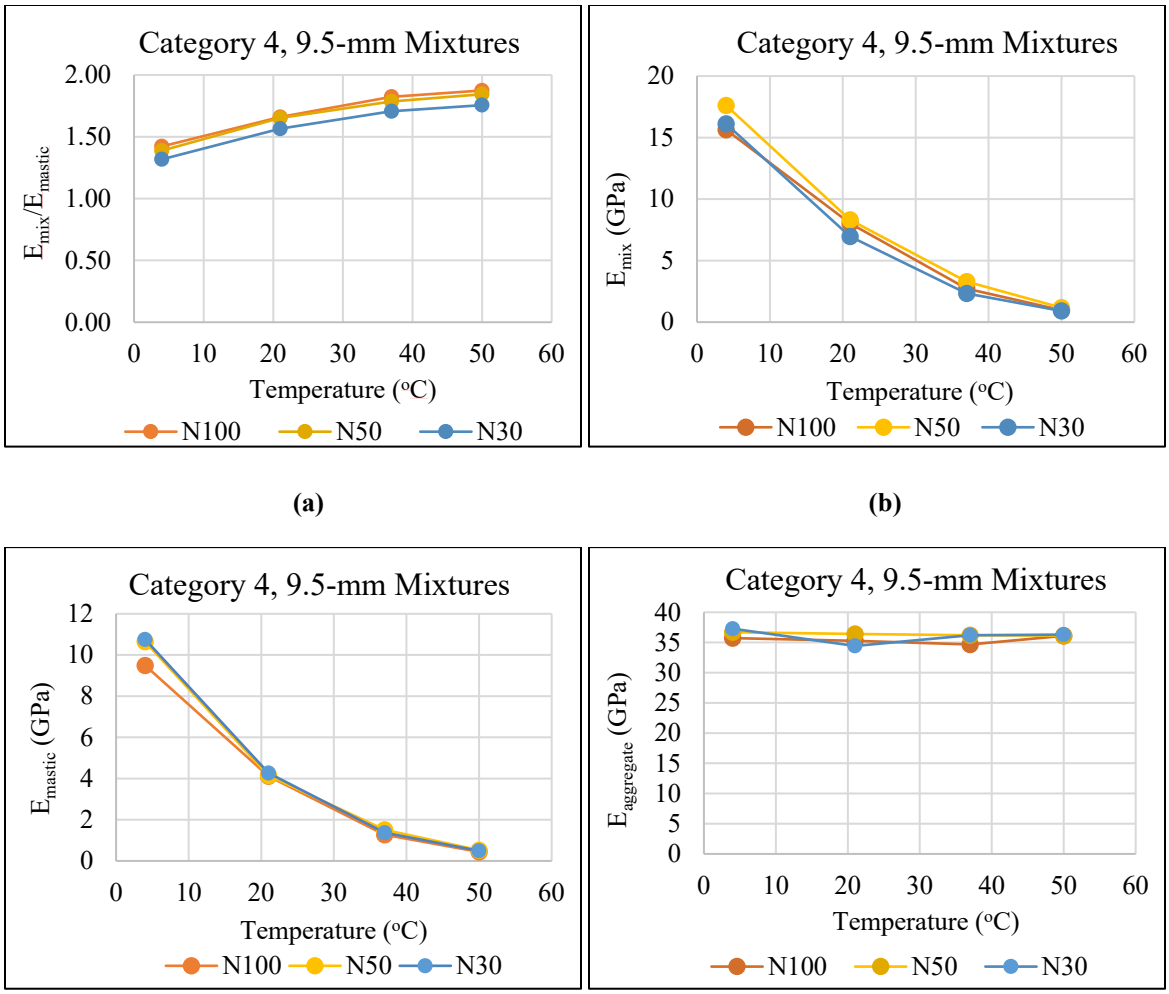

Figure 3-4 (a) Stiffness Ratio vs. Temperature for Category 4, 9.5-mm Mixtures, (b) Dynamic Modulus vs. Temperature, (c) Mastic Stiffness vs. Temperature, (d) Aggregate Stiffness vs. Temperature

Field Trials

The effect of different test and mixture conditions on the stiffness ratio can be interpreted from figures 3-5 and 3-6. Figure 3-5 shows the dynamic modulus and stiffness ratio of unaged mixtures, while figure 3-6 represents the values of aged mixtures. On comparing the results at aged and unaged conditions, at corresponding temperature and frequency, the stiffness ratio decreased with aging. This is because aging hardens the asphalt binder, which affects the mastic more than

the mixture. Hence, the change in E_{mastic} is more than the change in E_{mix} with aging, resulting in a lower stiffness ratio. Based on figures [3-5(a) and 3-5(b)] and [3-5(c) and 3-5(d)], the stiffness ratio decreased with frequency at both temperatures. Similarly, according to figures [3-5(a) and 3-5(c)] and [3-5(b) and 3-5(d)], the stiffness ratio increased with temperature at both frequency conditions. The same pattern was observed in the aged mixtures. These trends can be visualized from the elastic nature of an asphalt binder at low frequency/high temperature and the viscous nature at high frequency/low temperature. Hence, a mixture with a higher stiffness ratio is suitable for better cracking resistance, and a lower stiffness ratio is expected for a rut-resistant mixture.

Figures 3-7 and 3-8 present the inverse linear relationship between flow number and stiffness ratio for aged and unaged mixtures with a strong R^2 of around 0.8. The relationship between beam fatigue parameters and the stiffness ratio was not as expected (figures 3-9, 3-10); however, since the test results were ambiguous, additional testing is needed to draw the conclusions. A fair correlation could be established between the fracture energy and the stiffness ratio in figures 3-11 and 3-12, which explains the fatigue behavior.

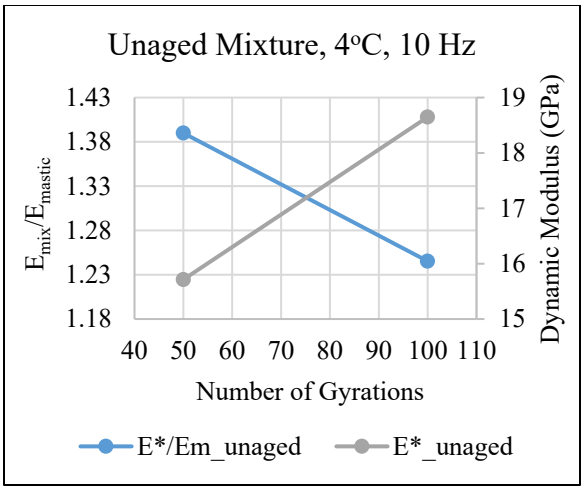

(a)

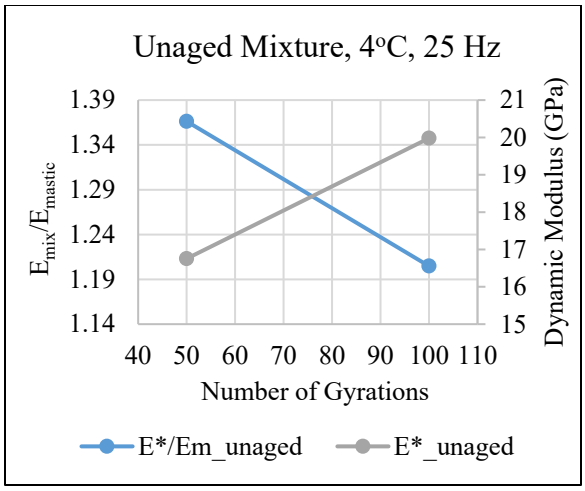

(b)

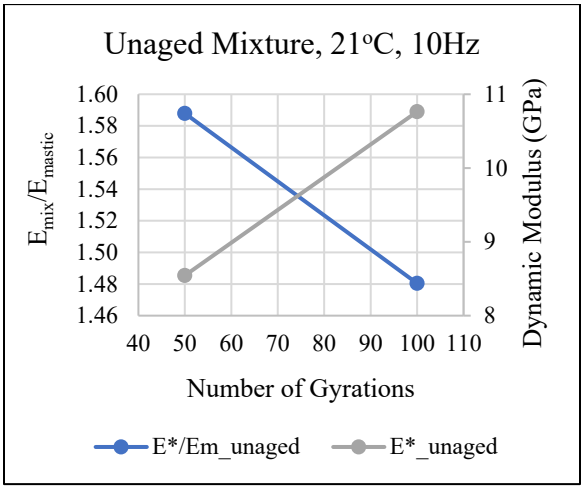

(c)

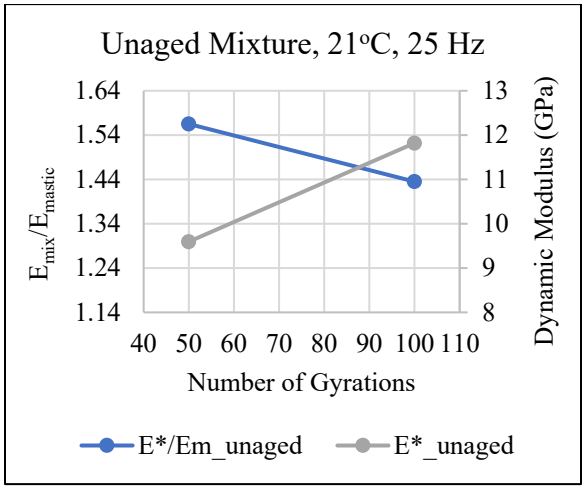

(d)

Figure 3-5 Example of Stiffness Ratio and Dynamic Modulus vs. Number of Gyrations for Unaged Mixtures at 4°C, 25°C and 10 Hz, 25 Hz Test Conditions

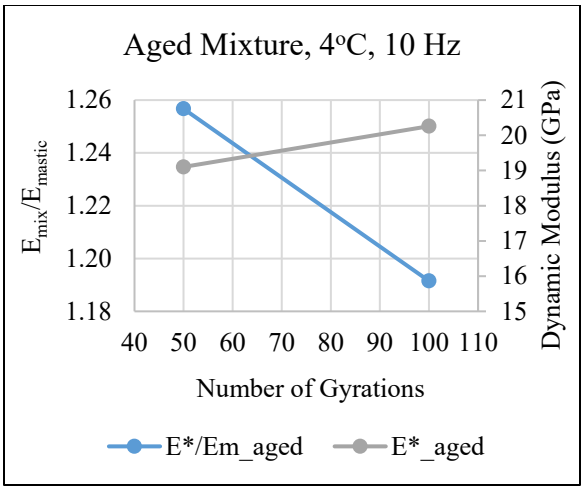

(a)

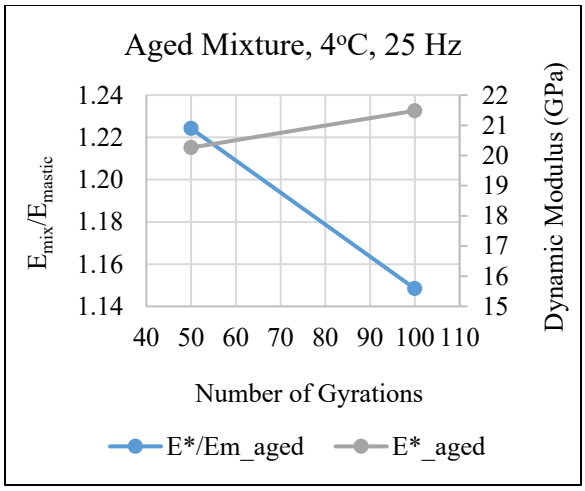

(b)

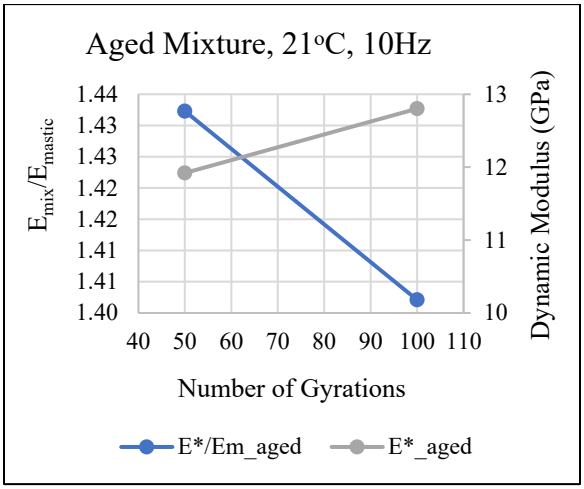

(c)

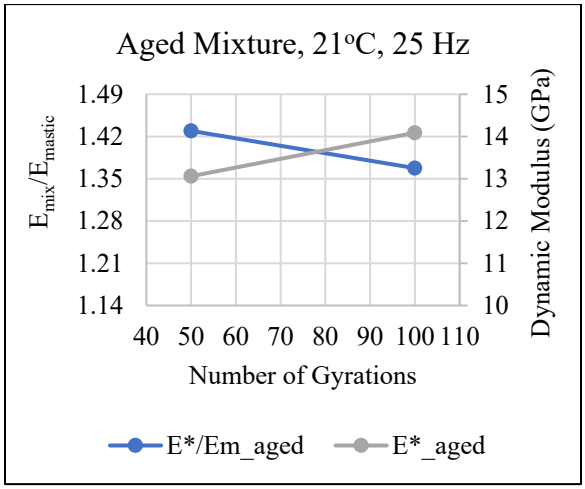

(d)

Figure 3-6 Example of Stiffness Ratio and Dynamic Modulus vs. Number of Gyrations for Aged Mixtures at 4°C, 25°C and 10 Hz, 25 Hz Test Conditions

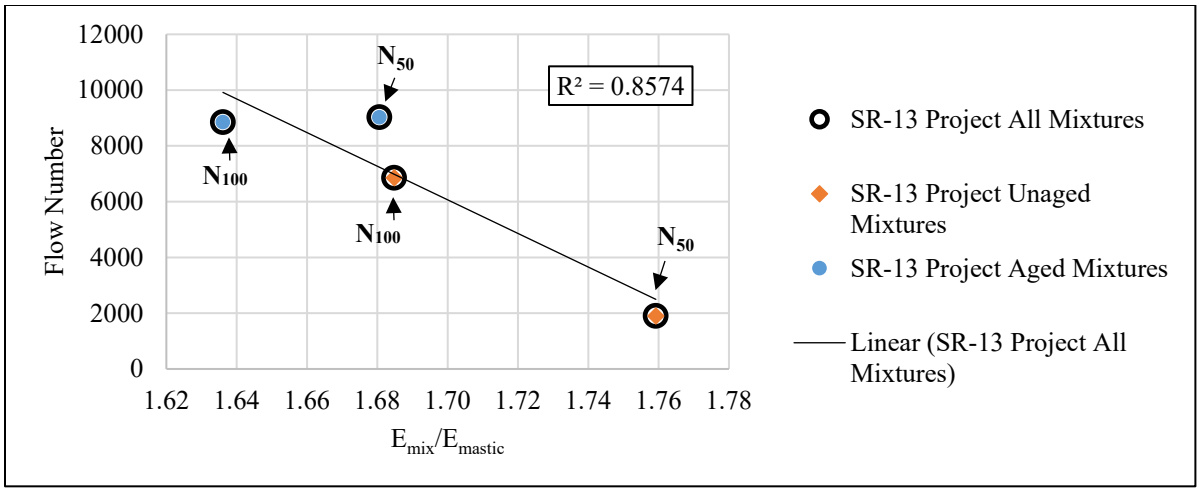

Figure 3-7 Correlation between the Flow Number and Stiffness Ratio for SR-13 Mixtures

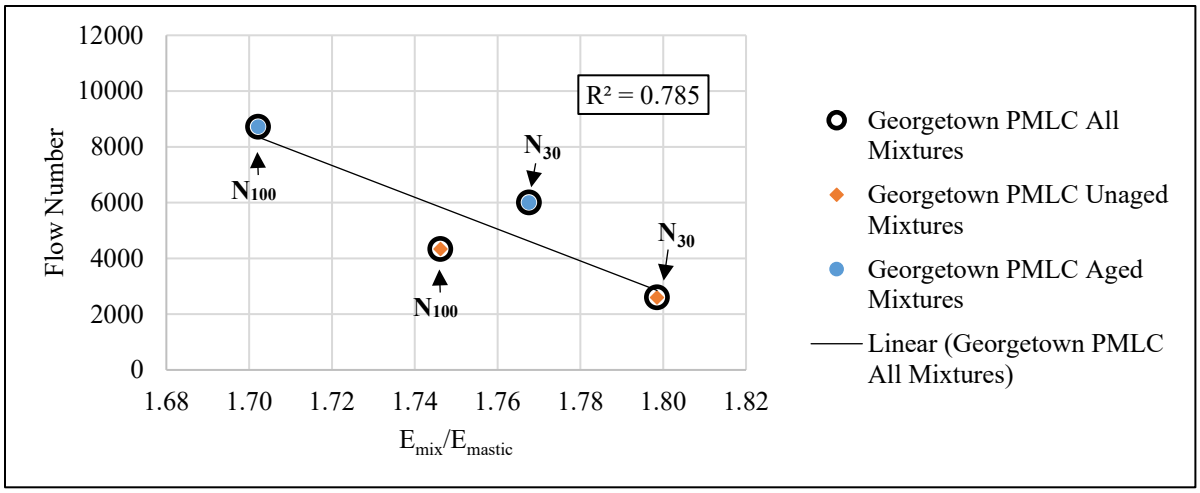

Figure 3-8 Correlation between the Flow Number and Stiffness Ratio for Georgetown PMLC Mixtures

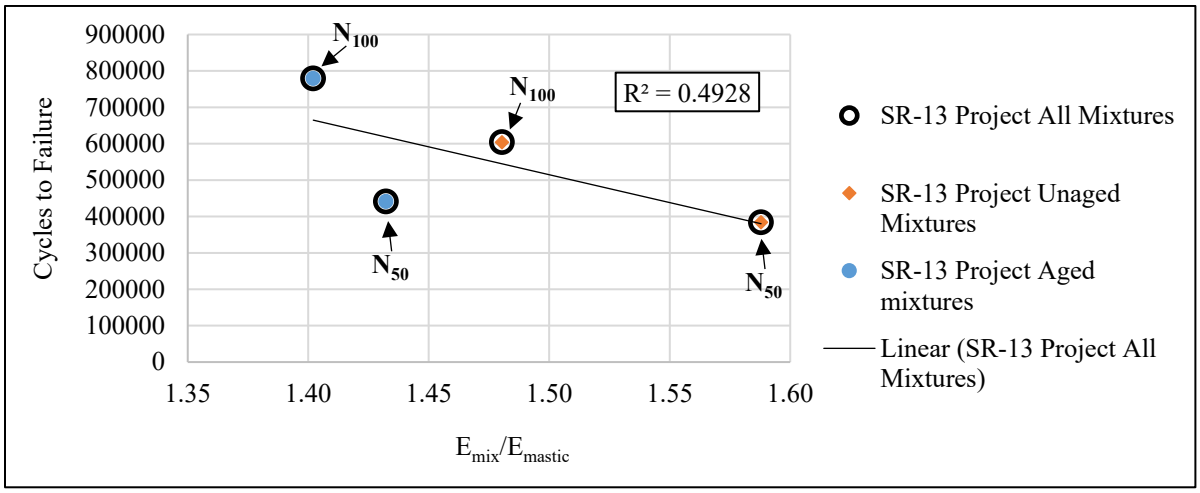

Figure 3-9 Correlation between the Beam Fatigue, Number of Cycles to Failure and Stiffness Ratio for SR-13 Mixtures

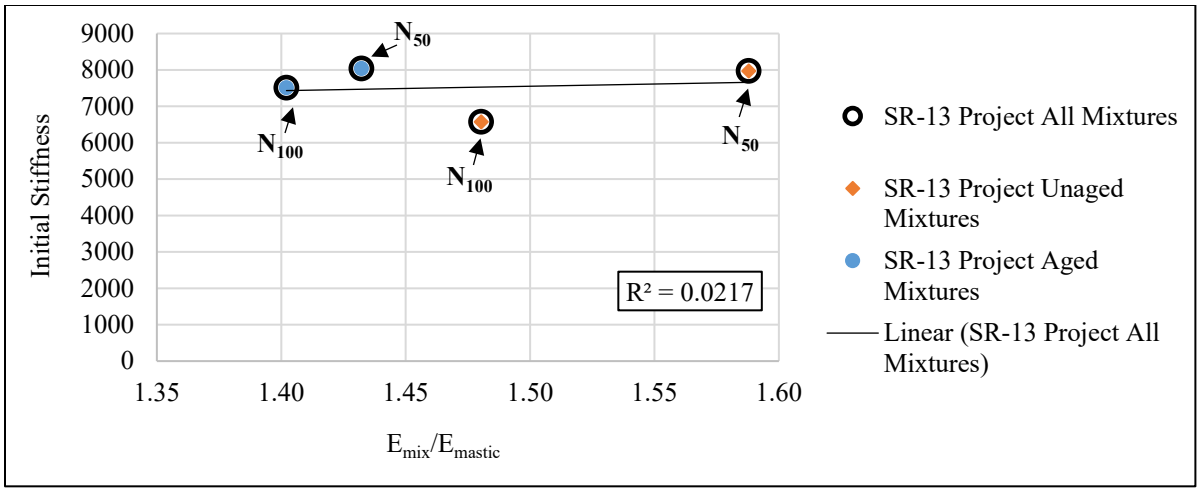

Figure 3-10 Correlation between the Beam Fatigue, Initial Stiffness and Stiffness Ratio for SR-13 Mixtures

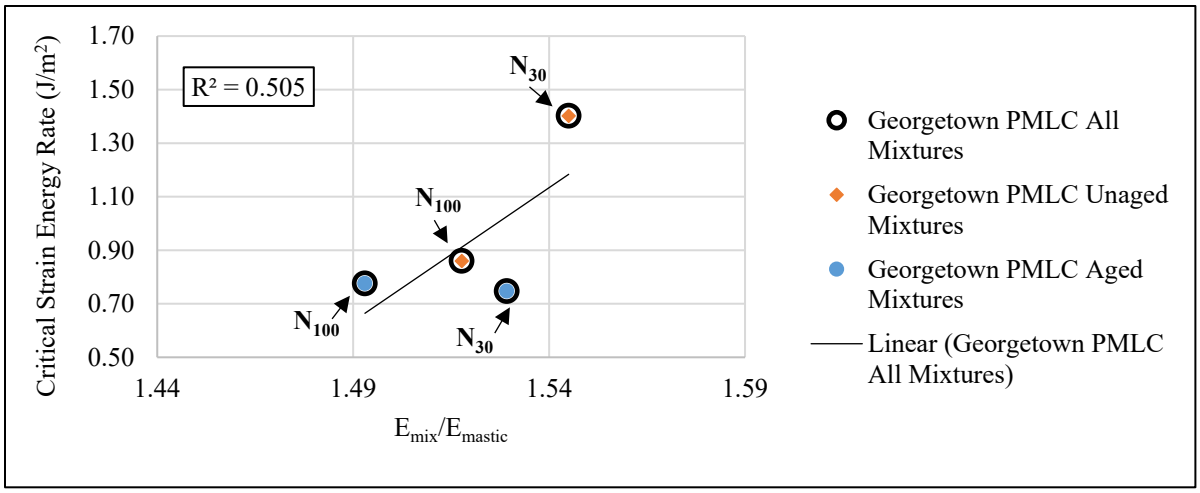

Figure 3-11 Correlation between the Strain Rate and Stiffness Ratio for Georgetown PMLC Mixtures

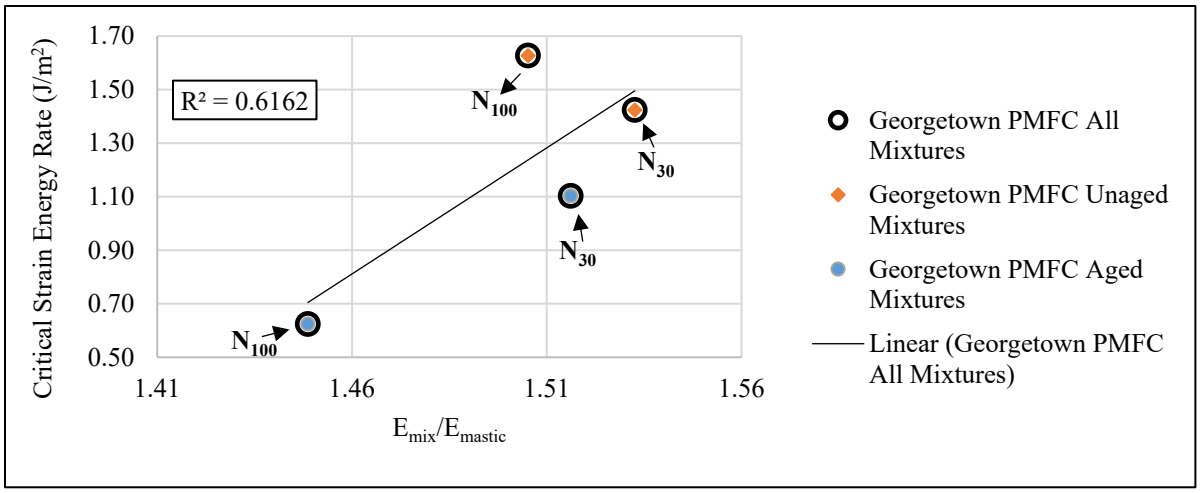

Figure 3-12 Correlation between the Strain Rate and Stiffness Ratio for Georgetown PMFC Mixtures

Conclusions

A new micromechanics-based performance indicator relating the stiffness of the mixture with that of the mastic was introduced in this section. The parameter was correlated with the stiffness, rutting, and fatigue performance of the plant mixed lab compacted mixtures. Satisfactory relationships were observed with R^2 of 0.8 for flow number and an R^2 of 0.5 for fracture strain energy, with the limited available data, concluding that the stiffness ratio could provide qualitative information about a mixture's pavement performance with only volumetrics and modulus testing. The sensitivity of the stiffness ratio was demonstrated by comparing the values calculated at different test conditions (temperatures, frequencies) and mixtures aging conditions. Based on the stiffness ratios calculated at different temperatures, it was found that 70 gyrations was optimal for Category 4, 19.0-mm re-designed mixtures, while 30 gyrations was suitable for Category 3, 9.5-mm and Category 4, 9.5-mm re-designed mixtures to achieve good permanent deformation characteristics.

CHAPTER IV

CALCULATION OF STIFFNESS RATIO FROM DYNAMIC MODULI OF DIFFERENT LABORATORY TESTS

In the entire Chapter 4, the stiffness ratios were calculated based on the AMPT dynamic modulus results. However, since the dynamic modulus of asphalt mixtures can be determined using a variety of test methods, a small analysis was conducted to assess the influence of the test methods on the stiffness ratio. The volume fractions of aggregate and mastic were calculated for the six mixtures described in Chapter 3. With these volume fractions and the air voids of the mixtures, the stiffness ratio analysis was performed twice for each mixture. First with cyclic test measurements and again with resonance test dynamic modulus values. Ideally, both the stiffness ratios should be identical as they represent the same mixture. This is affirmed in Figures 4-1 (a) to (f), where the stiffness ratios calculated with dynamic modulus values from the two test methods resulted in very similar values.

Hence, it adds to the advantages of using the stiffness ratio for evaluating a mixture, as it can mitigate the variations in the mechanical response of a mixture associated with the test method adopted and therefore better represent the mixture. Furthermore, the resonance test results can be successfully used in the model proposed by Onifade and Birgisson (2021).

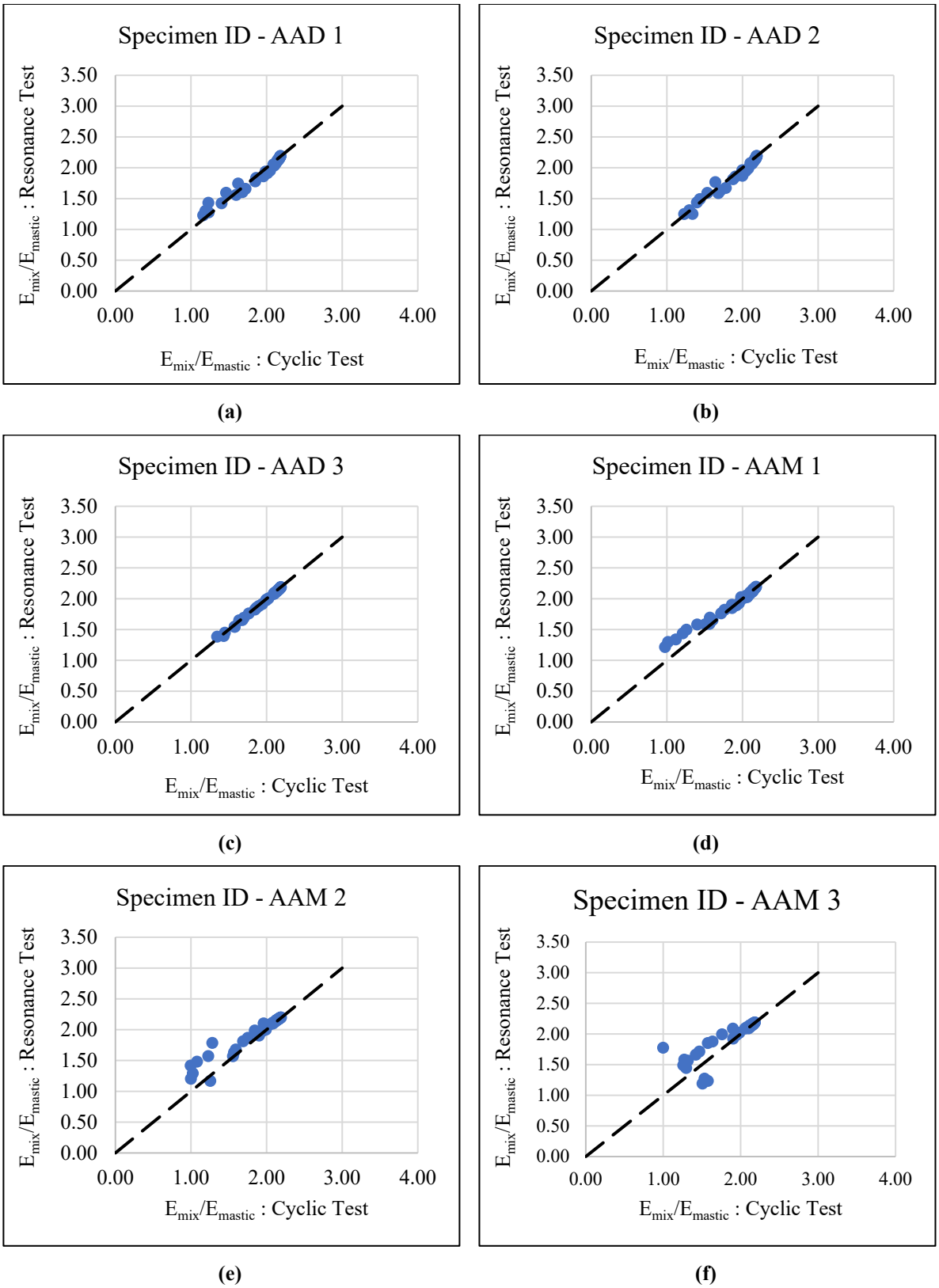

(a) **(b)** **(c)** **(d)** **(e)** **(f)**

Figure 4-1 Comparison of Stiffness Ratios Determined using the Cyclic Test and Resonance Test Results

CHAPTER V

SUMMARY AND CONCLUSIONS

This thesis investigated the potential of using the ratio of mixture and mastic modulus as a parameter to rank the asphalt mixture designs in terms of rutting and fatigue cracking performance. To begin with, two of the several laboratory methods available for determining the complex modulus of asphalt mixtures were examined. Two asphalt mixture designs were prepared using the same aggregate type and different binder types (AAD, AAM). The results from the cyclic AMPT test and the impact hammer resonance test on these specimens show that:

- At a low-frequency range of 0.01 Hz to 25 Hz, the dynamic modulus increases logarithmically with frequency and raises vertically with temperature. The phase angle increases with frequency until it reaches a peak and then decreases.
- At a high-frequency range of 8 kHz to 20 kHz, dynamic modulus increases at a much slower rate with frequency. The phase angle decreases linearly with an increase in the frequency.
- It was not possible to generalize the factor of difference between the dynamic modulus measurements from each testing method.
- For the AAD mixtures, the resonance test yielded a higher dynamic modulus and a lower phase angle than the cyclic test. The AAM mixtures showed the opposite pattern, with the dynamic modulus and phase angle from the resonance test being lower and higher, respectively, compared to the cyclic test results.
- The dynamic modulus measurements from the resonance test had a low relative standard deviation than the cyclic test for both mixture types.

- The phase angle measurements were inconsistent from both the tests, with the cyclic test producing slightly better results.

Master curves were developed following the existing AASHTO R 84 standard procedure. The cyclic test results could be fitted well with R^2 greater than 0.97 for all the mixtures. However, no optimum fit parameters were found to match the resonance test results. High-frequency measurements necessitate complex modulus models such as the HN model, 2S2P1D model, and others. The cyclic test fitted using the HN model showed that the HN model overestimated mixture stiffness at low frequencies, while the AASHTO R 84 model underestimated stiffness values at high frequencies. At intermediate frequencies, both models produced very similar dynamic modulus results. Nonetheless, the normalized root mean square deviation from the laboratory measurements was less than 8 percent for both models. Except for one mixture that had an 18 percent NRMSD, the resonance test results were successfully fitted with the HN model with NRMSD less than 10 percent. With operator training, the resonance test can be used to accurately characterize viscoelastic properties of asphalt mixtures at a faster rate (approximately 5 minutes for testing at a temperature and an hour for analysis) than the cyclic test. Further, the dynamic modulus of mixtures with different shapes like a disc, beam, etc., can also be determined using the resonance test (Gudmarsson 2014).

Next, the modulus of the individual mixture components was concentrated on. Based on the modulus of the mixture, the moduli of aggregates and mastic were back-calculated using the constrained non-linear multivariable optimization method. The equations were adopted from the model proposed by Onifade and Birgisson (2021). The ratio of the mixture stiffness and the mastic stiffness named the stiffness ratio was proposed as a new micromechanics-based performance parameter for characterizing the asphalt mixtures. The equations account for multiple phases in

the mixture, their volume fractions, viscoelastic properties of the binder, and the morphology of the aggregates. The comparative analysis performed inputting the cyclic, and the resonance test results into the model framework showed that both the modulus values result in similar stiffness ratios for a given mixture. Hence, this is a unique mixture-specific parameter.

The current Superpave mixture design method suggests target air voids of 4 percent for the laboratory asphalt mixtures and 7 percent for the performance test samples. This is to reflect the average field density requirement of 93 percent of the mixture's maximum theoretical specific gravity (G_{mm}). If field mixtures could be compacted to the same density as the laboratory mixture design, the pavement life could be increased by two to three years. With this objective, the Joint Transportation Research Program suggested a modified mixture design with the optimum binder content selected at 5 percent air voids. The percent binder and the voids in mineral aggregates were kept constant as the conventional Superpave mixture, and the aggregate gradation was changed to meet the requirements. The performance of mixtures prepared with different number of gyrations were evaluated to determine the optimum mixture designs for different traffic categories. The research was published as Report No. FHWA/IN/JTRP-2015/25 in 2015.

The final part of the thesis involved correlating the stiffness ratio with the pavement rutting and fatigue performance, using the post-field trial test results from the above study (Hekmatfar et al. 2015). The results show that the stiffness ratio has a strong inverse correlation with the flow number (R^2 of 0.8) and a fair direct correlation with the critical strain energy (R^2 of 0.5). Hence, a mixture with an optimal stiffness ratio would perform well in withstanding both rutting and fatigue distress. It was also established that the derived parameter was sensitive to mixture design, loading conditions, and aging. Based on the stiffness ratios of the re-designed mixtures determined at different temperatures and frequencies, 70 gyrations appeared to be the optimum for mixtures with

19.0-mm NMAS, and 30 gyrations seemed to be appropriate for 9.5-mm NMAS mixtures to produce a rut resistant design.

REFERENCES

AASHTO R 30. (2002). "Standard Practice for Mixture Conditioning of Hot Mix Asphalt (HMA)." American Association of State Highway and Transportation Officials, Washington, DC.

AASHTO R 84. (2017). "Standard Practice for Developing Dynamic Modulus Master Curves for Asphalt Mixtures Using the Asphalt Mixture Performance Tester (AMPT)." American Association of State Highway and Transportation Officials, Washington, DC.

AASHTO T 321. (2014). "Standard Method of Test for Determining the Fatigue Life of Compacted Asphalt Mixtures Subjected to Repeated Flexural Bending." American Association of State Highway and Transportation Officials, Washington, DC.

AASHTO T 342. (2011). "Standard Method of Test for Determining Dynamic Modulus of Hot Mix Asphalt (HMA)." American Association of State Highway and Transportation Officials, Washington, DC.

AASHTO T 378. (2017). "Standard method of test for determining the dynamic modulus and flow number for asphalt mixtures using the asphalt mixture performance tester (AMPT)." American Association of State Highway and Transportation Officials, Washington, DC.

AASHTO TP 124. (2018). "Standard Method of Test for Determining the Fracture Potential of Asphalt Mixtures using the Flexibility Index Test (FIT)." American Association of State Highway and Transportation Officials, Washington, DC.

AASHTO TP 79. (2013). "Determining the Dynamic Modulus and Flow Number for Hot Mix Asphalt (HMA) Using the Asphalt Mixture Performance Tester (AMPT)." American Association of State Highway and Transportation Officials, Washington, DC.

Ahmad, J., Hainin, M. R., Shaffie, E., Masri, K. A., and Shaffi, M. A. (2020). "Effect of temperature on phase angle and dynamic modulus of asphalt mixtures using SPT." *Materials Science Forum*, Vol. 1007, pp. 99-104, Trans Tech Publications Ltd.

Andrei, D., Witczak, M., W., and Mirza, M. W. (1999). "Development of Revised Predictive Model for the Dynamic (Complex) Modulus of Asphalt Mixtures. Development of the 2002 Guide for the Design of New and Rehabilitated Pavement Structures." NCHRP 1-37A, Interim Team Technical Report, Department of Civil Engineering, University of Maryland at College Park, MD.

ARA Inc., (2004). "Guide for mechanistic-empirical design of new and rehabilitated pavement structure, Part 2: Design Inputs, Chapter 2. Material Characterization." Draft Final Report 1-37A, National Cooperative Highway Research Program, Transportation Research Board, Washington, DC.

Bayane, B. M., Yang, E., and Yanjun, Q. (2017). "Dynamic modulus master curve construction using Christensen-Anderson-Marasteanu (CAM) model." *International Journal of Engineering Research and Applications*, 7(01), 53-63.

Bekele, A., Ryden, N., Gudmarsson, A., & Birgisson, B. (2019). "Automated Non-contact Resonance Excitation Method to Assess Low Temperature Dynamic Modulus of Asphalt Concrete." *Journal of Nondestructive Evaluation*, 38(2), 1-9.

Bennert, T. A. (2009). "Dynamic modulus of hot mix asphalt." Report No. FHWA-NJ-2009-011, Federal Highway Administration, U.S. Department of Transportation, Washington, D.C.

Bhasin, A., Button, J. W., and Chowdhury, A. (2003). "Evaluation of simple performance tests on HMA mixtures from the south central United States." Texas Transportation Institute, Texas A&M University System.

Bonaquist, R. (2016). “Critical factors affecting asphalt concrete durability.” Report No. 0092-14-06, Wisconsin Highway Research Program.

Bonaquist, R. F., Christensen, D. W., & Stump, W. (2003). “Simple performance tester for Superpave mix design: First-article development and evaluation.” *Transportation Research Board*, vol 513.

Boz, I. (2016). “Characterization of Asphalt Mixtures and Rap Binder Properties Through Impact Resonance Test.” Doctoral Dissertation, The Pennsylvania State University.

Christensen Jr, D. W., Pellinen, T., and Bonaquist, R. F. (2003). “Hirsch model for estimating the modulus of asphalt concrete.” *Journal of the Association of Asphalt Paving Technologists*, vol 72.

Clyne, T. R., Li, X., Marasteanu, M. O., and Skok, E. L. (2003). “Dynamic and resilient modulus of Mn/DOT asphalt mixtures.” Report MN/RC-2004-09, Minnesota Department of Transportation.

Cominsky, R. J., Huber, G. A., Kennedy, T. W., and Anderson, M. (1994). “The superpave mix design manual for new construction and overlays.” Report No. SHRP-A-407, Strategic Highway Research Program, Washington, DC.

Daniel, J. S., Chehab, G. R., & Kim, Y. R. "Issues affecting measurement of the complex modulus of asphalt concrete." *Journal of Materials in Civil Engineering*, 16.5 (2004): 469-476.

Dougan, C. E., Stephens, J. E., Mahoney, J., & Hansen, G. (2003). “E*-dynamic modulus test protocol: problems and solutions.” Report No. CT-SPR-0003084-F-03-3, University of Connecticut, Connecticut Transportation Institute.

FHWA. (2013). “Asphalt Mixture Performance Tester (AMPT)” https://www.fhwa.dot.gov/pavement/asphalt/pubs/hif13005.pdf

FHWA. (2020). “Asphalt Mixture Performance Tester (AMPT).” Retrieved from U.S. Department of Transportation Federal Highway Administration: https://www.fhwa.dot.gov/pavement/asphalt/tester.cfm

Gopalakrishnan, K., Kim, S., Ceylan, H., and Kaya, O. (2014). “Development of asphalt dynamic modulus master curve using falling weight deflectometer measurements.” Report No. IHRB Project TR-659, Iowa State University, Institute for Transportation.

Gudmarsson, A. (2014a). “Resonance testing of asphalt concrete.” Doctoral dissertation, KTH Royal Institute of Technology.

Gudmarsson, A., and Ryden, N. (2017). “Apps for modal analysis to characterize the complex modulus of asphalt concrete.” *Bearing Capacity of Roads, Railways and Airfields*, 209-215.

Gudmarsson, A., Ryden, N., and Birgisson, B. (2012). “Characterizing the low strain complex modulus of asphalt concrete specimens through optimization of frequency response functions.” *The Journal of the Acoustical Society of America*, 132(4), 2304-2312.

Gudmarsson, A., Ryden, N., Di Benedetto, H., and Sauzéat, C. (2015). “Complex modulus and complex Poisson’s ratio from cyclic and dynamic modal testing of asphalt concrete.” *Construction and Building Materials*, 88, 20-31.

Gudmarsson, A., Ryden, N., Di Benedetto, H., Sauzéat, C., Tapsoba, N., and Birgisson, B. (2014b). “Comparing linear viscoelastic properties of asphalt concrete measured by laboratory seismic and tension–compression tests.” *Journal of Nondestructive Evaluation*, 33(4), 571-582.

Hartmann, B., Lee, G. F., and Lee, J. D. (1994). “Loss factor height and width limits for polymer relaxations.” *The Journal of the Acoustical Society of America*, 95(1), 226-233.

Havriliak, S., and Negami, S. (1966). "A complex plane analysis of α-dispersions in some polymer systems." *Journal of Polymer Science Part C: Polymer Symposia*, Vol. 14, No. 1, pp. 99-117, New York: Wiley Subscription Services, Inc.

Hekmatfar, A., McDaniel, R. S., Shah, A., and Haddock, J. E. (2015). "Optimizing laboratory mixture design as it relates to field compaction to improve asphalt mixture durability." Report No. FHWA/IN/JTRP-2015/25, Purdue University.

Hu, J., Liu, P., and Steinauer, B. (2017). "A study on fatigue damage of asphalt mixture under different compaction using 3D-microstructural characteristics." *Frontiers of Structural and Civil Engineering*, 11(3), 329-337.

Jones, D. R. (1993). "SHRP materials reference library: Asphalt cements: A concise data compilation." Strategic Highway Research Program, National Research Council, Washington, DC, Vol. 1, p. 47.

Kim, Y. R., Underwood, B., Far, M. S., Jackson, N., Puccinelli, J., and Engineers, N. C. (2011). "LTPP computed parameter: dynamic modulus." Report No. FHWA-HRT-10-035, Federal Highway Administration, United States.

Kweon, G., & Kim, Y. R. (2006). "Determination of asphalt concrete complex modulus with impact resonance test." *Transportation Research Record*, 1970(1), 151-160.

Larcher, N., Takarli, M., Angellier, N., Petit, C., & Sebbah, H. (2015). "Towards a viscoelastic mechanical characterization of asphalt materials by ultrasonic measurements." *Materials and Structures*, 48(5), 1377-1388.

Levels, G. C. (2010). "Superpave Mix Design and Gyratory Compaction Levels." Technical Brief, FHWA-HIF-11-031, Federal Highway Administration.

Madigosky, W. M., Lee, G. F., and Niemiec, J. M. (2006). "A method for modeling polymer viscoelastic data and the temperature shift function." *The Journal of the Acoustical Society of America*, 119(6), 3760-3765.

Mirza, M. W., and Witczak, M. W. (1995). "Development of a Global Aging System for Short and Long Term Aging of Asphalt Cements." *Journal of the Association of Asphalt Paving Technologists*, Vol. 64, pp. 393-431.

Monismith, C. L., Alexander, R. L., and Secor, K. E. (1966). "Rheologic behavior of asphalt concrete." *Journal of Association Asphalt Paving Technologists*, Vol 35, pp. 400-450.

Mun, S. (2015). "Determining the dynamic modulus of a viscoelastic asphalt mixture using an impact resonance test with damping effect." *Research in Nondestructive Evaluation*, 26(4), 189-207.

Norambuena-Contreras, J., Castro-Fresno, D., Vega-Zamanillo, A., Celaya, M., & Lombillo-Vozmediano, I. (2010). "Dynamic modulus of asphalt mixture by ultrasonic direct test." *NDT & E International*, 43(7), 629-634.

Painter, P. C., and Coleman, M. M. (1997). "Fundamentals of Polymer Science – An Introductory Text." ISBN 1-56676-559-5, Technomic Publishing Co. Inc., Lancaster, PA.

Pellinen, T. K., Witczak, M. W., and Bonaquist, R. F. (2004). "Asphalt mix master curve construction using sigmoidal fitting function with non-linear least squares optimization." *Recent Advances in Materials Characterization and Modeling of Pavement Systems*, pp. 83-101.

Ryden, N. (2009). "Determining the asphalt mastercurve from free-free resonant testing on cylindrical samples." *Proceedings of the 7th International Symposium on Non-Destructive Testing in Civil Engineering (NDTCE09)*, Nantes, France.

Schwartz, C. W. (2005). “Evaluation of the Witczak dynamic modulus prediction model.” *CD-ROM, Presented at 84th Annual Transportation Research Board Meeting, Transportation Research Board*, Washington, D.C.

Solatifar, N., Kavussi, A., Abbasghorbani, M., and Katicha, S. W. (2019). “Development of dynamic modulus master curves of in-service asphalt layers using MEPDG models.” *Road Materials and Pavement Design*, 20(1), 225-243.

Sun, J. (2016). "Chapter 9—Predictions of rutting on asphalt pavements." Structural Behavior of Asphalt Pavements 17: 601-648.

Tauste, R., Moreno-Navarro, F., Gallego, R., & Rubio-Gámez, M. C. (2017). “Analysis of the sensitivity of the impact resonance frequency test as a tool to determine the elastic properties of bituminous materials.” *Materiales de Construcción*, 67(327), 131.

Tauste, R., Moreno-Navarro, F., Gallego, R., & Rubio-Gámez, M. C. (2017). “Analysis of the sensitivity of the impact resonance frequency test as a tool to determine the elastic properties of bituminous materials.” *Materiales de Construcción*, 67(327), 131.

Williams, M. L., Landel, R. F., and Ferry, J. D. (1955). “The temperature dependence of relaxation mechanisms in amorphous polymers and other glass-forming liquids.” *Journal of the American Chemical society*, 77(14), 3701-3707.

Williams, R. C. (2015). “Premature asphalt concrete pavement cracking.” Report No. FHWA-OR-RD-15-16, Oregon Department of Transportation Research Section.

Witczak, M. W. (2005). “Simple performance tests: Summary of Recommended Methods and Database.” National Cooperative Highway Research Program Report 547, Transportation Research Board, Washington, D.C.

Witczak, M. W., and Fonseca, O. A. (1996). "Revised predictive model for dynamic (complex) modulus of asphalt mixtures." *Transportation Research Record*, 1540(1), 15-23.

Witczak, M.W., Kaloush, K., Pellinen, T., El-Basyouny, M., and von Quintus, H. (2002). "Simple performance test for superpave mix design." National Cooperative Highway Research Program Report 465, Transportation Research Board, Washington, D.C.

Yusoff, N. I. M., Chailleux, E., and Airey, G. D. (2011b). "A comparative study of the influence of shift factor equations on master curve construction." *International Journal of Pavement Research and Technology*, 4(6), 324.

Yusoff, N. I. M., Shaw, M. T., and Airey, G. D. (2011a). "Modelling the linear viscoelastic rheological properties of bituminous binders." *Construction and Building Materials*, 25(5), 2171-2189.

Zhang, F., Wang, L., Li, C., and Xing, Y. (2020). "Predict the Phase Angle Master Curve and Study the Viscoelastic Properties of Warm Mix Crumb Rubber-Modified Asphalt Mixture." *Materials*, 13(21), 5051.

Zhang, J., Alvarez, A. E., Lee, S. I., Torres, A., and Walubita, L. F. (2013). "Comparison of flow number, dynamic modulus, and repeated load tests for evaluation of HMA permanent deformation." *Construction and Building Materials*, 44, 391-398.

Zhang, Y. (2012). "Anisotropic characterization of asphalt mixtures in compression." Doctoral dissertation, Texas A&M University, College Station.

Zhao, Y., Liu, H., Bai, L., and Tan, Y. (2013). "Characterization of linear viscoelastic behavior of asphalt concrete using complex modulus model." *Journal of Materials in Civil Engineering*, 25(10), 1543-1548.